Mathematical analysis of a porous-media model for rock-dehydration processes

Andrea Zafferi* **Marita Thomas†**

February 24, 2023

Abstract

We discuss a nonlinear parabolic set of equations for reactive two-phase flows with applications in geosciences to rock dehydration processes. We prove existence of solutions for this model starting from a fully discretized system and subsequently pass to the continuous limit. The assumptions here made are based on real life data.

Keywords and phrases. Reactive porous media, Darcy flow, time-discrete scheme, existence of solutions.

1 Introduction

Rock hydration processes are within the most relevant phenomena for the earth water cycle. Hydration processes may occur when water in contact with exhumed oceanic litosphere bounds chemically to mineral phases, i.e., Olivine, to form new hydrated material, i.e., serpentinite. Subsequently in Earth water cycle we encounter dehydration processes that occur when hydrated rocks are subducted and the steady increase of temperature triggers chemical reactions through which water is again released and, due to the lower density, spring back to the surface. There is evidence [vKHSA11] that this mechanism of water liberation has to be very efficient to keep pace with the subduction rate and it is thought to happen on several stages. The inital stages are the porosity formation caused by fluid liberation and the fluid flow through the rock matrix with transport of chemical compounds that might further trigger dehydration reactions. In this work we are concered with the analysis of a model describing those phenomena.

A first model for reaction induced porosity-formation applied to serpentinites is to be found in [PJP+17]. This model features Darcy flow in a dehydrated (porous) medium and an expression for the porosity which results from chemical reactions and the assumption of conservation of non-volitile mass density

$$\partial_t \left(\rho_{\mathrm{s}}(1-\phi)+\rho_{\mathrm{f}}\phi\right) = \nabla\cdot\left(\rho_{\mathrm{f}}K(\phi)\nabla\pi\right)\,, \tag{1a}$$

$$\partial_t \left(\rho_{\mathrm{s}}(1-X_{\mathrm{h}})(1-\phi)\right) = 0\,, \tag{1b}$$

where ρ_{s}, resp. ρ_{f}, represents the solid, resp. fluid, mass density, ϕ the porosity or volume fraction of the fluid phase, π is the pressure and $K(\phi)$ denotes a Kozeny-Carman-type permeability. From (1b) one can infer

$$\phi = 1-\frac{\rho_{\mathrm{s}}^0(1-X_{\mathrm{h}}^0)(1-\phi^0)}{\rho_{\mathrm{s}}(1-X_{\mathrm{h}})}\,, \tag{1c}$$

with X_{h} being the weight percentage of fluid content in the solid phase while a^0 will denote from now on the initial condition for any quanity a. This reduces in fact the PDE system (1) to one single evolution

*Freie Universität Berlin, Arnimalle 9, 14195 Berlin, Germany. Email: andrea.zafferi@fu-berlin.de

†Freie Universität Berlin, Arnimalle 9, 14195 Berlin, Germany. Email: marita.thomas@fu-berlin.de

equation (1a) for the total mass density $\rho_{\text{tot}} = (\rho_{\text{s}}(1-\phi) + \rho_{\text{f}}\phi)$. In recent years the model was extended to include diffusive phenomena, see e.g., [BJV+20, HVJ22]. More specifically, the system of equations reads:

$$\partial_t \left(\rho_{\text{s}}(1-\phi) + \rho_{\text{f}}\phi\right) = \nabla \cdot \left(\rho_{\text{f}} K(\phi)\nabla\pi\right) , \tag{2a}$$

$$\partial_t \left(\rho_{\text{s}} c_{\text{s}}(1-\phi) + \rho_{\text{f}} c_{\text{f}}\phi\right) = \nabla \cdot \left(\rho_{\text{f}} c_{\text{f}} K(\phi)\nabla\pi + \rho_{\text{f}} c_{\text{f}}\phi D_c \nabla c_{\text{f}}\right) , \tag{2b}$$

complemented with an analytical expression for the porosity ϕ which accounts for the concentration of specific species as well, cf. (1c):

$$\phi = 1 - \frac{\rho_{\text{s}}^0(1 - c_{\text{s}}^0 - X_{\text{h}}^0)(1-\phi^0)}{\rho_{\text{s}}(1 - c_{\text{s}} - X_{\text{h}})} , \tag{2c}$$

where c_{s}, resp. c_{f}, denotes the content of a given species, i.e., Si, of the solid (s), resp. fluid (f), phase and D_c in (2b) represents the diffusion coefficient. Observe that (2b) describes the time variation of the total mass of a given species Z, since $\rho_Z = \rho_{\text{s}} c_{\text{s}}(1-\phi) + \rho_{\text{f}} c_{\text{f}}\phi$. In this paper we will focus on existence results for the systems (1) and (2). Although we will be discussing mainly model (2), the same strategy applies to (1). Assumptions and main differences will be explored in Sec. 2. A derivation of these equations goes beyond the scope of this work nonetheless we refer to [BJV+20] for the derivation using standard conservation laws and flux definitions or to [ZHP+22] for a variational formulation and reduction strategies based on the GENERIC formalism.

From the applications point of view, equations (1a) and (2a)-(2b) are solved numerically for the unknowns π and (π, c_{s}) respectively, whereas the remaning quantities c_{f}, X_{h}, ρ_{i}, with $\text{i} \in \{\text{s}, \text{f}\}$, depend implicitely on the unknowns and on the (given) temperature θ. Throughout this paper we will consider θ constant and thus will not have a direct impact on our results. However we keep this dependency in the notation to highlight that the thermodynamic equilibrium on which the functions c_{f}, X_{h}, $\rho_{\text{s}}, \rho_{\text{f}}$ are computed changes accordingly.

To fix ideas, a typical dehydration reaction we will be studying is the following

$$(\text{Mg}, \text{Fe})_{48}\text{Si}_{34}\text{O}_{85}(\text{OH})_{62} \rightleftharpoons 34(\text{Mg}, \text{Fe})_2\text{SiO}_4 + 31\text{H}_2\text{O} + 10{\text{SiO}_2}^{\text{aq}} ,$$

where antigorite (hydrous mineral) is transformed into olivine (non-hydrous mineral) and a fluid composed by water and a small amount of silica. We note that many other dehydration reactions are possible, however, a complete discussion of those goes beyond the scope of this paper. With this in mind, we observe that equation (2b) describes the evolution of the total mass of Silicon (Si). Furthermore, this sets restrictions to the range of values of temperature θ, pressure π and solid concentration c_s, namely, we have a temperature range of $400 - 500°\text{C}$,, a pressure within $0.8 - 2$ GPa and the concentration within $17 - 20$ weight percentage of solid phase.

In order to better use tools from analysis we observe that the systems (1) and (2) can be rephrased in parabolic form. We perform this reformulation in section 2 and discuss the assumptions on the systems comparing with thermodynamical data. Alltogether, PDEs systems (1) and (2) can be rewritten as

$$\partial_t \boldsymbol{\rho} - \nabla \cdot (\mathbb{M}(\boldsymbol{\rho})\nabla\boldsymbol{\rho}) = 0 \qquad \text{in } (0, \text{T}) \times \Omega , \tag{3a}$$

$$\boldsymbol{\rho} = g \qquad \text{on } [0, \text{T}] \times \Gamma_{\text{D}} , \tag{3b}$$

$$\mathbb{M}\nabla\boldsymbol{\rho} \cdot \nu = h \qquad \text{on } [0, \text{T}] \times \Gamma_{\text{N}} , \tag{3c}$$

$$\boldsymbol{\rho}(0) = \boldsymbol{\rho}_0 \qquad \text{in } \Omega , \tag{3d}$$

where $\boldsymbol{\rho} = \rho_{\text{tot}}$ for (1) and $\boldsymbol{\rho} = (\rho_{\text{tot}}, \rho_{\text{Si}0_2})^\top$ for (2). The initial data is denoted by $\boldsymbol{\rho}_0$ and $\mathbb{M}(\boldsymbol{\rho}) = (\mathbb{M}_{\text{ij}}(\boldsymbol{\rho}))_{\text{ij}}$ with $\text{i}, \text{j} \in \{\text{t}, \text{s}\}$ is a scalar, cf. (1), or a 2×2 matrix for (2). Equations (3b) and (3c) are the inhomogenous Dirichlet and Neumann boundary conditions acting on the boundary Γ_{D} and $\Gamma_{\text{N}} := \partial\Omega \backslash \Gamma_{\text{D}}$, respectively. With a proper extension of the Dirichlet datum onto the domain, i.e., $g \in H^1(\Omega)$ it is possible to reformulate the problem with homogeneous Dirichelet boundary conditions by introducing $\boldsymbol{\rho}_g := \boldsymbol{\rho} - g$ and solving for $\boldsymbol{\rho}_g$. From now on we will not make the distinction between homogeneous and inhomogenous Dirichlet boundary conditions anymore and will assume that this transformation of the equations is always possible. Based on that, we define the space

$$V := H^1_{\text{D}}(\Omega) = \left\{ v \in H^1(\Omega) \,:\, v = 0 \text{ a.e. on } \Gamma_{\text{D}} \right\} , \tag{4}$$

which we will be using for the parabolic form of (1), while for (2) we will use $\boldsymbol{V} := V \times V$. Throughout this paper we denote the duality product between a space $\boldsymbol{W}$ and its dual $\boldsymbol{W}^*$ by $\langle \cdot, \cdot \rangle_{\boldsymbol{W}^* \times \boldsymbol{W}}$, or simply $\langle \cdot, \cdot \rangle_{\boldsymbol{W}}$, and by omitting the subscript we refer to the duality product in V, resp. $\boldsymbol{V}$. Similarly the norm is denoted by $\| \cdot \|_V$, resp. $\boldsymbol{V}$. It is then possible to introduce a suitable weak formulation of the porous media equation (1a):

Definition 1.1. *Let* $\mathrm{T} > 0$ *and* $\Omega \subset \mathbb{R}^d$ *be a bounded Lipschitz domain. Let* $Q_\mathrm{T} := (0, \mathrm{T}) \times \mathbb{R}^d$ *be the time-space cylinder. Given a function* $\rho_\mathrm{tot} : [0, \mathrm{T}] \to V$ *we define the following weak formulation for every test function* $v \in V$*:*

$$\int_{Q_\mathrm{T}} \dot{\rho}_\mathrm{tot}(t)\, v + \mathbb{M}(\rho_\mathrm{tot}(t)) \nabla \rho_\mathrm{tot}(t) \cdot \nabla v \,\mathrm{d}x \,\mathrm{d}t - \int_0^\mathrm{T} \int_{\Gamma_\mathrm{N}} v|_{\Gamma_\mathrm{N}} h \,\mathrm{d}\mathcal{H}^{d-1} \,\mathrm{d}t = 0\,, \tag{5}$$

where $\mathcal{H}^{d-1}$ *denotes the* $(d-1)$*-dimensional Hausdorff measure.*

Similarily for (2) we have

Definition 1.2. *Let* $\mathrm{T} > 0$ *and* $\Omega \subset \mathbb{R}^d$ *be a bounded Lipschitz domain. Let* $Q_\mathrm{T} := (0, \mathrm{T}) \times \mathbb{R}^d$ *be the time-space cylinder. Given a function* $\boldsymbol{\rho} = (\rho_\mathrm{tot}, \rho_{\mathrm{Si}0_2}) : [0, \mathrm{T}] \to \boldsymbol{V}$ *we define the following weak formulation for every test function* $\boldsymbol{v} \in \boldsymbol{V}$*:*

$$\int_{Q_\mathrm{T}} \dot{\boldsymbol{\rho}}(t)\, \boldsymbol{v} + \hat{\mathbb{M}}(\boldsymbol{\rho}(t)) \nabla \boldsymbol{\rho}(t) \cdot \nabla \boldsymbol{v} \,\mathrm{d}x \,\mathrm{d}t - \int_0^\mathrm{T} \int_{\Gamma_\mathrm{N}} \boldsymbol{v}|_{\Gamma_\mathrm{N}} h \,\mathrm{d}\mathcal{H}^{d-1} \,\mathrm{d}t = \boldsymbol{0}\,. \tag{6}$$

This paper is so structered: in sec. 2 we present a parabolic reformulation of systems (1) and (2), validate and discuss properties and assumptions on the systems with thermodynamic dataset. In the succeeding section 3 we provide a time- and space-discrete schemes of the parabolic equations and prove the existence of discrete solutions. Finally, in sections 4 and 5 we perform limit passages from discrete to continuous setting, henche proving existence of solutions.

2 Reformulation, notation and basic assumptions

In this section we explore the basic assumptions on models (1) and (2) providing physical data to support them. We reformulate the two systems in terms of a new set of variables that clarifies the classification of these into parabolic type equations. The reformulation will be then used in the following sections to prove analytical results.

2.1 Parabolic form of system (1)

Although system (1) proved to be convenient for numerical implementations, we reformulate it to show its parabolic nature and relative properties. We observe that time integration of (1b) leads to the expression (1c). Moreover it is assumed that $\rho_\mathrm{s}, \rho_\mathrm{f}, X_\mathrm{h}$ are given functions of pressure π and temperature θ. We will not consider variations of temperature here and therefore will assume that θ is constant over the whole domain at any time. However, we highlight here the system dependency on θ since mineral phases stability and hence $\rho_\mathrm{s}, \rho_\mathrm{f}, X_\mathrm{h}$ are susceptible to temperature changes. A constant temperature assumption is often made in geology [**?**] since temperature equilibration and fluid flows usually happen on different time scales. Based on that we have

Assumption 2.1. *The functions* $\rho_\mathrm{s} = \tilde{\rho}_\mathrm{s}(\pi, \theta), \rho_\mathrm{f} = \tilde{\rho}_\mathrm{f}(\pi, \theta), X_\mathrm{h} = \tilde{X}_\mathrm{h}(\pi, \theta)$ *are given functions of pressure* π *and temperature* θ*.*

Although being explicitely unknowns, values can be recovered from look-up tables [VP22]. An example of these functions is given in figure 1. Additionally, from now on throughout this paper we will use a tilde to distinguish between a function $\tilde{a}$ and its value a.

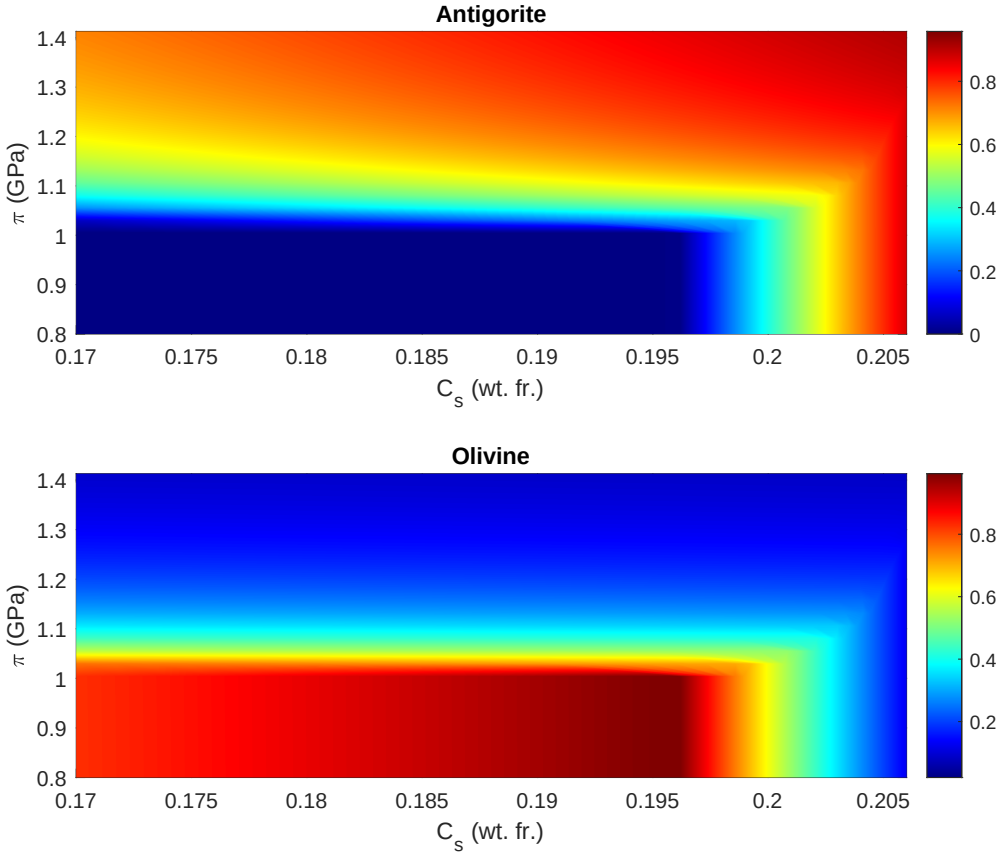

Based on 2.1 together with (1c) we consider the porosity as a function of pressure and temperature

$$\phi = 1 - \frac{\rho_{\mathrm{s}}^0(1 - X_{\mathrm{h}}^0)(1 - \phi^0)}{\rho_{\mathrm{s}}(1 - X_{\mathrm{h}})} := \tilde{\phi}(\pi, \theta)\,. \tag{7}$$

Similarly the total mass density appearing in (1a) can be rewritten as $\tilde{\rho}_{\mathrm{tot}}(\pi,\theta) := \tilde{\rho}_{\mathrm{f}}(\pi,\theta)\tilde{\phi}(\pi,\theta) + \tilde{\rho}_{\mathrm{s}}(\pi,\theta)(1-\tilde{\phi}(\pi,\theta))$ and the Darcy coefficient $\tilde{K}_D(\pi,\theta) := \tilde{\rho}_{\mathrm{f}}(\pi,\theta)K(\tilde{\phi}(\pi,\theta))$ so that equation (1a) reads

$$\partial_t \tilde{\rho}_{\mathrm{tot}} = \nabla \cdot \left(\tilde{K}_D(\pi,\theta)\nabla\pi \right)\,. \tag{8}$$

Now we assume that

Assumption 2.2. *For every $\theta > 0$ fixed, the function $\tilde{\rho}_{\mathrm{tot}}(\cdot,\theta)$ is invertible in π, the inverse function $\tilde{\rho}_{\mathrm{tot}}^{-1}(\cdot,\theta)$ is continuously differentiable, and there are constants $0 < c_\star < c^\star$ such that*

$$\frac{1}{c^\star} < \partial_\rho \tilde{\rho}_{\mathrm{tot}}^{-1}(\rho,\theta) = \frac{1}{\partial_\pi \tilde{\rho}_{\mathrm{tot}}(\tilde{\rho}_{\mathrm{tot}}^{-1}(\rho,\theta),\theta)} < \frac{1}{c_\star}\,. \tag{9}$$

Thus, for every $\theta > 0$ we find

$$\pi = \tilde{\pi}(\rho_{\mathrm{tot}},\theta) := \tilde{\rho}_{\mathrm{tot}}^{-1}(\rho_{\mathrm{tot}},\theta)\,. \tag{10}$$

By assuming the temperature θ to be constant in space and using the chain rule for differentiation, from (10) we calculate

$$\nabla\pi = \nabla\tilde{\pi}(\rho_{\mathrm{tot}},\theta) = \partial_{\rho_{\mathrm{tot}}}\tilde{\pi}(\pi,\theta)\nabla\rho_{\mathrm{tot}} = \frac{1}{\partial_\pi \tilde{\rho}_{\mathrm{tot}}(\tilde{\pi}(\rho_{\mathrm{tot}},\theta))}\nabla\rho_{\mathrm{tot}}\,.$$

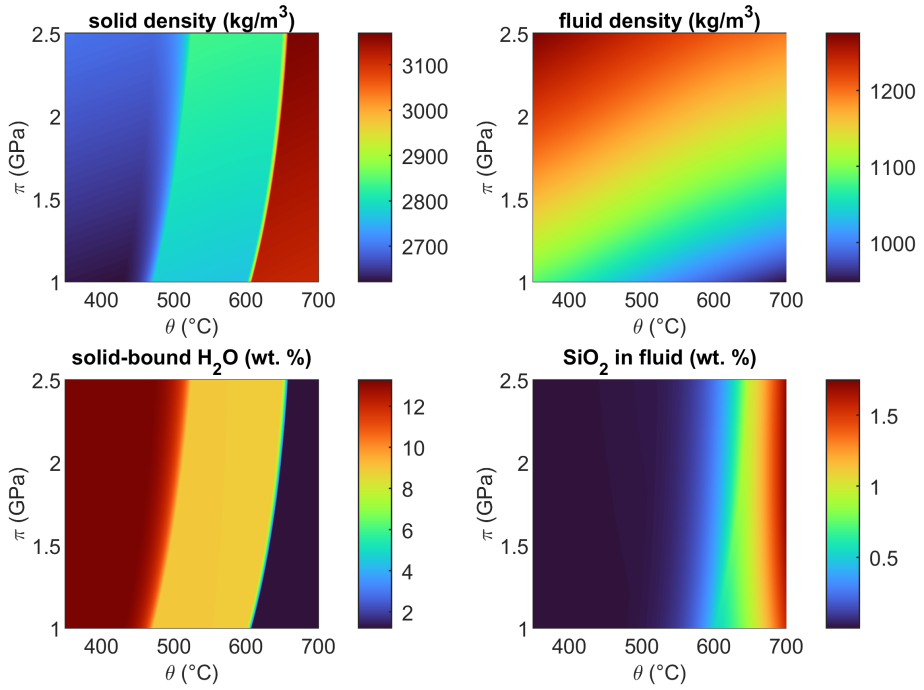

Figure 1: Pressure-temperature dependence of solid density, fluid density, solid-bound H_2O content and fluid composition wrt. SiO_2 for a typical serpentinite bulk rock composition as also used in the model of [HVJ22]. Their model uses these pre-computed values as lookup tabels to close the system of equations.

This gives the relation

$$\tilde{K}_{\mathrm{D}}(\pi,\theta)\nabla\pi = \hat{K}_{\mathrm{D}}(\rho_{\mathrm{tot}},\theta)\nabla\rho_{\mathrm{tot}} \qquad \text{with} \quad \hat{K}_{\mathrm{D}}(\rho_{\mathrm{tot}},\theta) = \frac{\tilde{K}_{\mathrm{D}}(\tilde{\pi}(\rho_{\mathrm{tot}},\theta),\theta)}{\partial_\pi \rho_{\mathrm{tot}}(\tilde{\pi}(\rho_{\mathrm{tot}},\theta),\theta)}\,.$$

Hence, (1a) can be rewritten as a parabolic equation for the total mass density ρ_{tot}

$$\partial_t \rho_{\mathrm{tot}} = \nabla\cdot\left(\hat{K}_{\mathrm{D}}(\rho_{\mathrm{tot}},\theta)\nabla\rho_{\mathrm{tot}}\right)\,. \tag{11}$$

Furthermore, for $\hat{K}$ we make the following assumptions

Assumption 2.3. *For every $\theta > 0$ fixed, the function $\hat{K}(\rho_{\mathrm{tot}},\theta)$ is continuous and there are constants $0 < \hat{k}_\star < \hat{k}^\star$ such that $\hat{k}_\star \le \hat{K}(\rho_{\mathrm{tot}},\theta) \le \hat{k}^\star$ for all $\rho_{\mathrm{tot}} \in \mathbb{R}$.*

We now discuss the validity of the assumptions recently made with numerical examples implemented using a thermodynamicly consisten mineral dataset.

2.1.1 Perusal of assumptions (2.2) & (2.3) for thermodynamical rock data

In the following we validate the mathematical assumptions (2.2) and (2.3) with the thermodynamical rock data used in [PJP+17]. Figure 2 shows the total mass density $\rho = \tilde{\rho}(\pi)$ as a function of pressure π in its geologically relevant range of 0.8-2 GPa. Fig. 2 confirms that $\tilde{\rho}$ is a continuous and strictly monotone function of pressure π, hence bijective. Yet, it also turns out that the map suffers from a kink at $\pi = 1.2$ GPa, which hampers the assumption of continuous differentiability of $\tilde{\rho}$ and its inverse $\tilde{\rho}^{-1}$, cf. (2.2). Indeed, this kink coincides with a phase transformation between antigorite and olivine as shown is Fig. 1 and in Fig. 1. It therefore also appears in the porosity $\phi = \tilde{\phi}(\pi,\theta)$ and in the coefficient function $\tilde{K}(\pi,\theta)$ at $\pi = 1.2$ GPa, see Fig. 3. As expected this translates into a discontinuity of the coefficient function $\hat{K}(\cdot,\theta)$ at $\rho \approx 2600$ kg/m^3. We further point out that the porosity shown in Fig.3 is strictly positive and bounded from below by the value $\tilde{\phi}(2\mathrm{GPa}, 480°\mathrm{C}) = 0.035 > 0$. In turn, we find the coefficient function

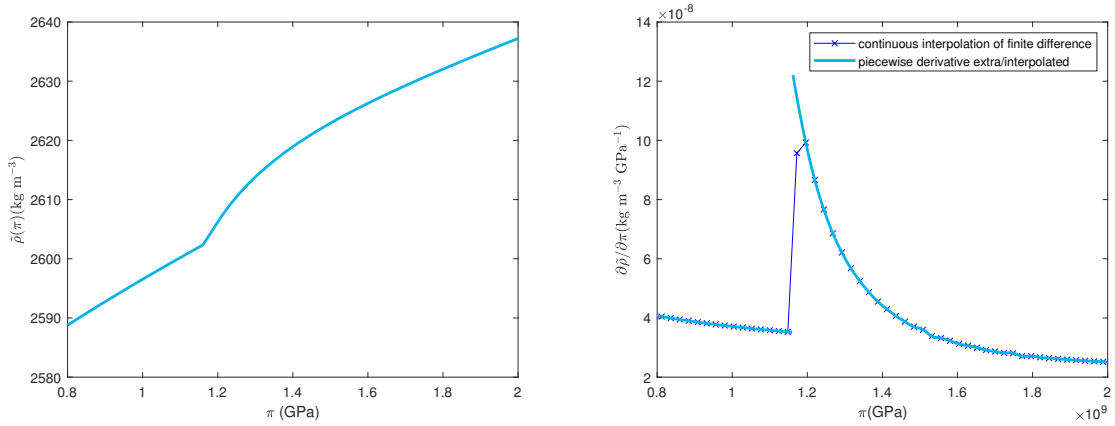

Figure 2: on the left: Example of $\tilde{\rho} = \tilde{\rho}(\pi, \theta)$ for a given composition and at fixed temperature of 480°C. One can see the continuity and strict monotonicity of $\tilde{\rho}$ which in return guarantee the existence of a continuous inverse $\tilde{\rho}^{-1}$. On the right: plot of the derivative $\partial\tilde{\rho}/\partial\pi$ for two possible discretizations. It can bee seen that it is discontinuous around $\pi = 1.2$GPa and that is bounded from below and above satisfying globally but one point assumption (2.2).

$\hat{K}(\cdot, \theta)$ to be uniformly bounded from above and from below by a value strictly larger than zero, so that assumption (2.3) is satisfied.

As the violation of the continuity assumptions, cf. (2.3), for $\hat{K}(\cdot, \theta)$ and (2.2) are concerned, we point out that the analytical results given in Thm. **??**, 2. predict that the weak solution $\rho(t, \cdot)$ for all $t \in [0, \mathrm{T}]$ stays confined between values $0 < r_* < r^*$ a.e. in Ω, if the initial datum ρ_0 is chosen with this property. In other words, if the initial datum is chosen with values strictly below or strictly above the critical value of $\rho = 2600$ kg/m^3 (corresponding to the critical pressure of 1.2 GPa), then also the solution will not exceed this value apart from a set of zero measure at any later time $t \in (0, \mathrm{T}]$. Thus, under this additional assumption on the initial datum, all the assumptions (2.2) and (2.3) are met and therefore existence of a unique weak solution is guaranteed by Thm. **??**, 1. However, this also means that in this setting the phase transition, with ρ exceeding the critical value on sets of positive measure, cannot be described by Thm. **??** using the original thermodynamical data set. Instead, in order to cover also this case, one would have to mollify $\tilde{\rho}(\cdot, \theta)$ and $\hat{K}(\cdot, \theta)$ in a small neighbourhood of the non-smoothness. From a geological perspective, even though the interesting pressure range is between 0.8-2 GPa, it is very difficult for a geological system to experience this complete range. Usually, pressure variations are very small and π is confined to a neighborhood of a certain value. Therefore it is usually sufficient to study one of either areas below or above 1.2 GPa. Additionally let us point out that the phase stability, hence the position of the kink, varies with temperature and rock composition: If the system has a high iron content, one would find this kink in the mass density for higher values of pressure, cf. [**?**]. As explained in Fig. 1 for the composition and temperature of this specific example, antigorite, the hydrated rock, is stable for pressure values above 1.2 GPa and olivine, the dehydrated rock, is stable at pressure values below 1.2 GPa. In conclusion, since the interest lies in the investigation of the dehydration process, we can confine the analysis to the regime below 1.2 GPa.

2.2 Parabolic form of system (2)

The main difference between these two system, as remarked previously, is the addition of diffusion phenomena, in our case specifically connected to the silica SiO_2 content, which requires the addition of a new variable c_s and although the application of a similar approach as the one used in Section 2.1 might seem straightforward, the thermodynamical data behind the model (15) hide a series of challenges that require a special treatment. We dedicate this section to their description.

As before, we assume that

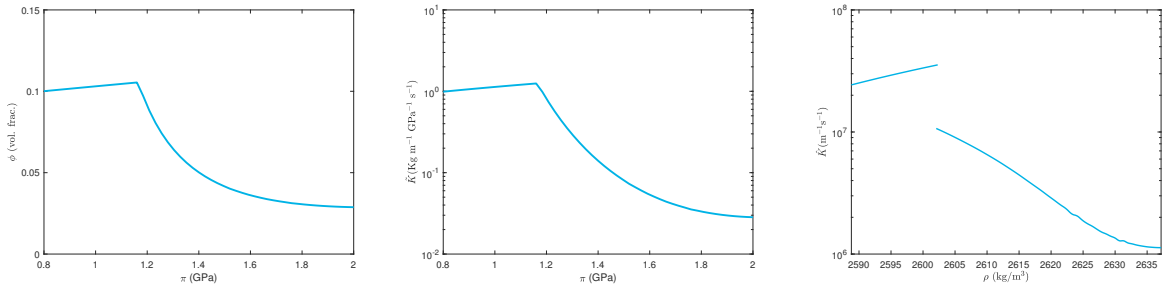

Figure 3: Example of $\phi = \phi(\pi, \theta), \hat{K}(\pi, \theta)$ and $\tilde{K}(\pi, \theta)$ for a given composition and at fixed temperature of 480°C. For these simulations we have set ratio between permeability of the medium and viscosity of the fluid $\hat{K}/\mu = 1$. Thus, positivity and continuity of $\hat{K}$ relies on ϕ, which never reaches zero.

Assumption 2.4. *The functions $\rho_{\mathrm{s}} = \tilde{\rho}_{\mathrm{s}}(\pi, c_{\mathrm{s}}, \theta), \rho_{\mathrm{f}} = \tilde{\rho}_{\mathrm{f}}(\pi, c_{\mathrm{s}}, \theta), X_{\mathrm{h}} = \tilde{X}_{\mathrm{h}}(\pi, c_{\mathrm{s}}, \theta)$ are given functions of pressure π, concentration c_{s} and temperature θ.*

Again their analytical form is unknown, but their values can be determined from thermodynamical data tables. Combining assumption 2.4 with (2c) the porosity ϕ can be understood as a function of the variables $(\pi, c_{\mathrm{s}}, \theta)$ as follows

$$\phi = 1 - \frac{\rho_{\mathrm{s}}^0(1 - c_{\mathrm{s}}^0 - X_{\mathrm{h}}^0)(1 - \phi^0)}{\rho_{\mathrm{s}}(1 - c_{\mathrm{s}} - X_{\mathrm{h}})} =: \tilde{\phi}(\pi, c_{\mathrm{s}}, \theta)\,. \tag{12}$$

Based on this we introduce the notation

$$\tilde{\rho}_{\mathrm{tot}}(\pi, c_{\mathrm{s}}, \theta) = \tilde{\rho}_{\mathrm{s}}(\pi, c_{\mathrm{s}}, \theta)(1 - \tilde{\phi}(\pi, c_{\mathrm{s}}, \theta)) + \tilde{\rho}_{\mathrm{f}}(\pi, c_{\mathrm{s}}, \theta)\tilde{\phi}(\pi, c_{\mathrm{s}}, \theta)\,, \tag{13a}$$

$$\tilde{\rho}_{\mathrm{Si}}(\pi, c_{\mathrm{s}}, \theta) = \tilde{\rho}_{\mathrm{s}}(\pi, c_{\mathrm{s}}, \theta)(1 - \tilde{\phi}(\pi, c_{\mathrm{s}}, \theta))\tilde{c}_{\mathrm{f}}(\pi, c_{\mathrm{s}}, \theta) + \tilde{\rho}_{\mathrm{f}}(\pi, c_{\mathrm{s}}, \theta)\tilde{\phi}(\pi, c_{\mathrm{s}}, \theta)c_{\mathrm{f}}\,, \tag{13b}$$

$$\tilde{K}_{\mathrm{D}}(\pi, c_{\mathrm{s}}, \theta) = \tilde{\rho}_{\mathrm{f}}(\pi, c_{\mathrm{s}}, \theta)K(\pi, c_{\mathrm{s}}, \theta)\,, \tag{13c}$$

$$K(\pi, c_{\mathrm{s}}, \theta) = \frac{\kappa}{\mu}\tilde{\phi}^3(\pi, c_{\mathrm{s}}, \theta)\,, \tag{13d}$$

$$\tilde{D}_c(\pi, c_{\mathrm{s}}, \theta) = \tilde{\rho}_{\mathrm{f}}(\pi, c_{\mathrm{s}}, \theta)\tilde{\phi}(\pi, c_{\mathrm{s}}, \theta)D_c\,, \tag{13e}$$

where the coefficients κ, μ and D_c are the permeability, fluid viscosity and diffusion coefficient respectively and are assumed to be positive constants. Equations (2a) and (2b) can then be rewritten as follows:

$$\partial_t\tilde{\rho}_{\mathrm{tot}}(\pi, c_{\mathrm{s}}, \theta) = \mathrm{div}\left(\tilde{K}_{\mathrm{D}}(\pi, c_{\mathrm{s}}, \theta)\nabla\pi\right)\,, \tag{14a}$$

$$\partial_t\tilde{\rho}_{\mathrm{Si}}(\pi, c_{\mathrm{s}}, \theta) = \mathrm{div}\left(\tilde{c}_{\mathrm{f}}(\pi, c_{\mathrm{s}}, \theta)\tilde{K}_{\mathrm{D}}(\pi, c_{\mathrm{s}}, \theta)\nabla\pi + \tilde{D}_c(\pi, c_{\mathrm{s}}, \theta)\nabla\tilde{c}_{\mathrm{f}}(\pi, c_{\mathrm{s}}, \theta)\right)\,, \tag{14b}$$

This is a PDE system of the form

$$\partial_t\tilde{\boldsymbol{\rho}}(\boldsymbol{q}, \theta) - \mathrm{div}\left(\tilde{\mathbb{M}}(\boldsymbol{q}, \theta)\nabla\boldsymbol{q}\right) = 0 \quad \text{with} \tag{15a}$$

$$\boldsymbol{q} := \begin{pmatrix}\pi \\ c_{\mathrm{s}}\end{pmatrix} \quad \tilde{\boldsymbol{\rho}} := \begin{pmatrix}\tilde{\rho}_{\mathrm{tot}} \\ \tilde{\rho}_{\mathrm{Si}}\end{pmatrix} \quad \tilde{\mathbb{M}} := \begin{pmatrix}\tilde{K}_{\mathrm{D}} & 0 \\ \tilde{c}_{\mathrm{f}}\tilde{K}_{\mathrm{D}} + \tilde{D}\partial_\pi\tilde{c}_{\mathrm{f}} & \tilde{D}_c\partial_{c_{\mathrm{s}}}\tilde{c}_{\mathrm{f}}\end{pmatrix}\,. \tag{15b}$$

where we have used the chain rule $\nabla\tilde{c}_{\mathrm{f}}(\pi, c_{\mathrm{s}}, \theta) = \partial_\pi\tilde{c}_{\mathrm{f}}(\pi, c_{\mathrm{f}}, \theta) + \partial_{c_{\mathrm{s}}}\tilde{c}_{\mathrm{f}}(\pi, c_{\mathrm{f}}, \theta)$. Now we set

$$\boldsymbol{\rho} = \tilde{\boldsymbol{\rho}}(\boldsymbol{q}, \theta)\,, \tag{16}$$

and make the following assumptions on the map $\tilde{\boldsymbol{\rho}}$ and its inverse

Assumption 2.5. *For every $\theta > 0$ fixed, the function $\tilde{\boldsymbol{\rho}}(\cdot, \theta)$ is continuously differentiable and invertible in $\boldsymbol{q}$ and the inverse $\tilde{\boldsymbol{\rho}}^{-1}(\cdot, \theta)$ is continuously differentiable.*

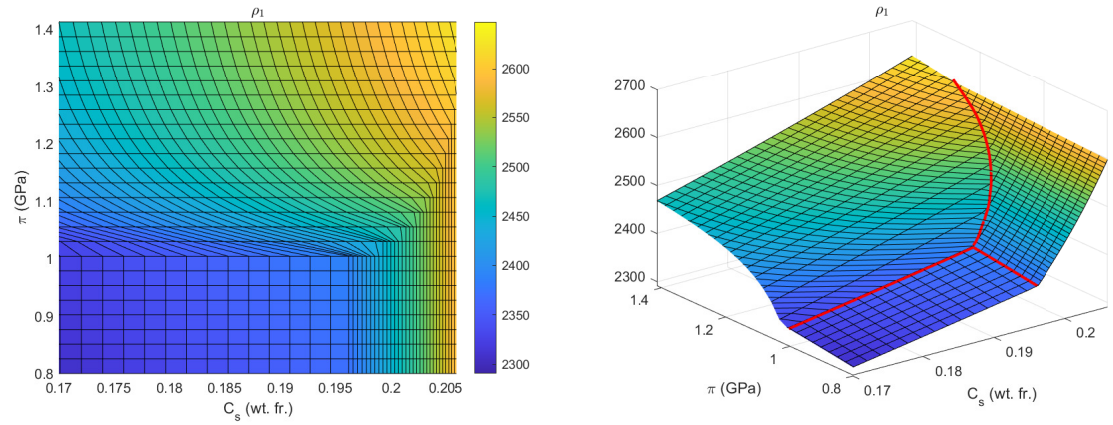

Figure 4: Plots of the total mass density $\tilde{\rho}_1 = \tilde{\rho}_1(\pi, c_s, \theta)$. On the left a 2D plot showing the discretization grid resulting from an interpolation of the thermodynamic dataset. The non-differentiability points are marked with a red line in the right plot. This shows the division into three main areas ($(0.8, 1)$GPa $\times$ $(0.17, 0.196), (0.8, 1)$GPa $\times$ $(0.196, 0.2)$ and the remaining part of the domain) delimited by two straight lines and one curve with a contact point around $(1\text{GPa}, 0.195)$. These three subdivisions and the values for which $\tilde{\rho}_1$ is continuous but not differentiable are more clearly seen in the 3D plot on the right.

We note that assumptions 2.5 amount to the following conditions

$$\begin{aligned} &\textit{For all } \theta > 0 \textit{ the Jacobian } \mathrm{D}_{\boldsymbol{q}}\tilde{\boldsymbol{\rho}}(\cdot,\theta) = \begin{pmatrix} \partial_\pi \tilde{\rho}_1(\cdot,\theta) & \partial_{c_s}\tilde{\rho}_1(\cdot,\theta) \\ \partial_\pi \tilde{\rho}_2(\cdot,\theta) & \partial_{c_s}\tilde{\rho}_2(\cdot,\theta) \end{pmatrix} \textit{ is continuous with} \\ &\det \mathrm{D}_{\boldsymbol{q}}\tilde{\boldsymbol{\rho}}(\boldsymbol{q},\theta) > 0 \textit{ for all admissible } \boldsymbol{q} \in \mathbb{R}^2\,, \textit{ and also} \\ &\mathrm{D}_{\boldsymbol{\rho}}\tilde{\boldsymbol{\rho}}^{-1}(\cdot,\theta) = \mathrm{D}_{\boldsymbol{q}}\tilde{\boldsymbol{\rho}}(\tilde{\boldsymbol{\rho}}^{-1}(\cdot,\theta),\theta)^{-1} \textit{ is a continuous function in } \boldsymbol{\rho}\,. \end{aligned} \tag{17a}$$

Then we have

$$\boldsymbol{q} = \tilde{\boldsymbol{\rho}}^{-1}(\boldsymbol{\rho},\theta) =: \tilde{\boldsymbol{q}}(\boldsymbol{\rho},\theta)$$

and the system (15) can be rewritten as a parabolic PDE system of the form

$$\partial_t \boldsymbol{\rho} - \nabla \cdot \left(\hat{K}_{\mathrm{D}}(\boldsymbol{\rho},\theta)\nabla\boldsymbol{\rho} \right) = 0\,, \tag{18}$$

where we used the relations

$$\nabla \boldsymbol{q} = \partial_{\boldsymbol{\rho}}\tilde{\boldsymbol{\rho}}(\boldsymbol{\rho},\theta)\nabla\boldsymbol{\rho} \qquad \text{and} \qquad \hat{K}_{\mathrm{D}}(\boldsymbol{\rho},\theta) := \tilde{K}(\tilde{\boldsymbol{q}}(\boldsymbol{\rho},\theta),\theta)\partial_{\boldsymbol{\rho}}\tilde{\boldsymbol{q}}(\boldsymbol{\rho},\theta)\,.$$

Now we state the following assumptions on $\hat{K}_{\mathrm{D}}$

Assumption 2.6. *For every $\theta > 0$ the matrix $\hat{K}_{\mathrm{D}}$ has the following properties:*

- *$\hat{K}_{\mathrm{D}}(\cdot,\theta) : \mathbb{R}^2 \to \mathbb{R}^{2\times 2}$ is continuous,*
- *$\hat{K}_{\mathrm{D}}(\boldsymbol{q},\theta) : \mathbb{R}^{2\times 2} \to \mathbb{R}^{2\times 2}$ is bounded and positively definite uniformly w.r.t. $(\boldsymbol{q},\theta)$, i.e., there are constants $0 < K_\star < K^\star$ s.th. for all $(\boldsymbol{q},\theta)$ and all $\boldsymbol{v} \in \mathbb{R}^2$ there holds:*

$$K_\star |\boldsymbol{v}|^2 < \boldsymbol{v} \cdot \hat{K}_{\mathrm{D}}(\boldsymbol{q},\theta)\boldsymbol{v} < K^\star |\boldsymbol{v}|^2\,. \tag{19}$$

2.2.1 Perusal of assumptions (17) & (2.6) for thermodynamical rock data

Firstly we recall that system (15) is written in terms of $\boldsymbol{q} = (\pi, c_s)^\top$, i.e., in terms of the pressure π and the concentration of silica in the solid c_s. A close inspection of the thermodynamical rock data sets reveals that the introduction of this additional complexity causes the resulting mass densities to have regions of non-invertibility and non-differentiability, as it can be seen in Figures 4 and 5 for the mass densities $\tilde{\rho}_1$

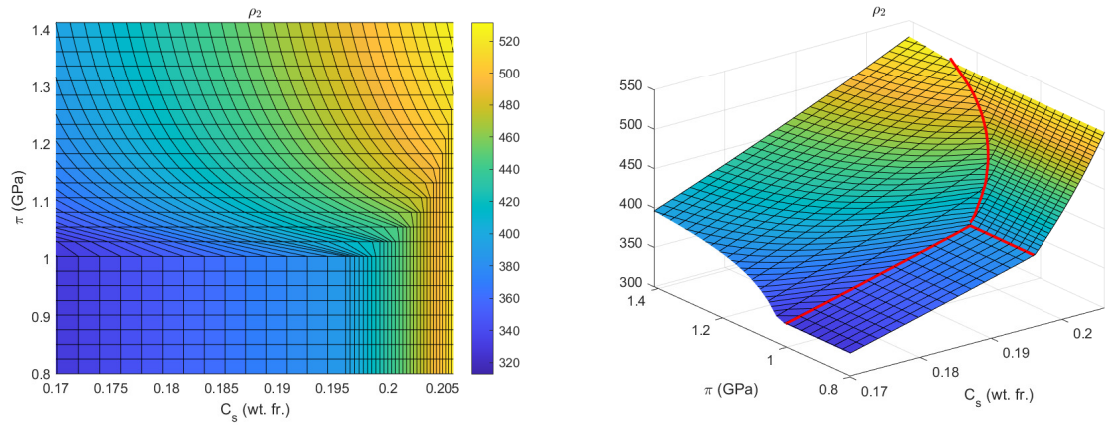

Figure 5: Plots of the total mass density of silica $\tilde{\rho}_2 = \tilde{\rho}_2(\pi, c_s, \theta)$. On the left a 2D plot showing the discretization grid resulting from an interpolation of the thermodynamic dataset. The non-differentiability points are marked with a red line in the right plot. This shows the division into three main areas (the same of $\tilde{\rho}_1$ shown in Figure 4). These three subdivisions and the values for which $\tilde{\rho}_2$ is continuous but not differentiable are more clearly seen in the 3D plot on the right.

and $\tilde{\rho}_2$. This is in analogy to the kink in the thermodynamical data of model (1) shown in Fig. 3. More precisely, we see in Fig. 4 that the total mass density $\tilde{\rho}_1$ is strictly monotonously increasing with respect to pressure and silica-content, but that kinks arise in the region of the antigorite-olivine phase transition discussed in Fig. 1. Similarly, also Fig. 5 shows a monotone behavior of the total silica-mass density $\tilde{\rho}_2$ in pressure and silica-content, also with kinks arising at the antigorite-olivine phase transition. Obviously, within this region assumptions (**??**) and (17) are not satisfied.

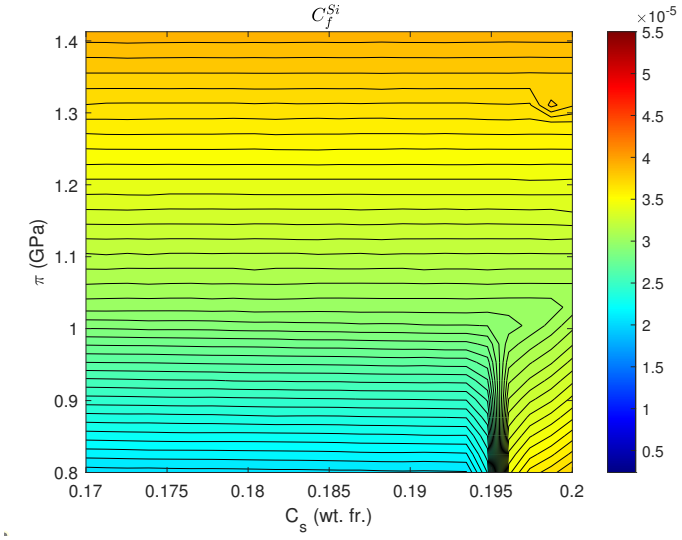

Figure 6: The figure shows isolevels for the function $\tilde{c}_f(\pi, \tilde{c}_s)$ at $\theta = 480°C$. One can see that in most parts of the considered domain we have $\partial c_f / \partial c_s = 0$ which translates to no diffusion occurring in the system. However it is worth noticing that there is a small area in the bottom right corner where this condition is not met. In addition, a discontinuity point where the lines are more dense can be seen around $c_s \approx 0.195$. This discontinuity would, i.e., invalidates assumption (**??**)

Additionally we point out that in (15) the gradient of the silica concentration in the fluid $\tilde{c}_f$ drives the diffusion process. Hence, it would be natural to chose $\tilde{c}_f$ as a variable. However, as Fig. 6 reveals,

in wide areas of the data range $\tilde{c}_\mathrm{f}$ is constant with respect to c_s, so that the function is not invertible in these areas. This is the reason why system (2) is written in terms of the variables π and c_s. Indeed, such plateau regions followed by kinks as in Fig. 6 are common in thermodynamical rock data sets. They are also predicted in [Guy93] in the case of non-convex thermodynamical functions, which is again closely related to phase stability.

As can be seen from (15), in regions where $\partial\tilde{c}_\mathrm{f}/\partial c_\mathrm{s} = 0$, diffusion of silica is absent and the mathematical classification of the PDE system becomes unclear. Similar to Section 2.1.1 one may also try here to confine the initial data to a data range that ensures the validity of assumptions (17) and (2.6). Then the results of Theorem **??** would also guarantee that solutions are confined to that data range for all times $t \in (0, T]$. However, as can be seen from (15) the positive definiteness of $\hat{K}_\mathrm{D}$, and hence the classification of the PDE system, is not solely linked to the positive definiteness of the Jacobian $\mathrm{D}_{\boldsymbol{q}}\tilde{\boldsymbol{\rho}}$ but also to the values of the material constants κ, μ, and D_c contributing to the non-symmetric coefficient matrix $\tilde{K}$ in (15). These material constants are, in fact, the main contributors, together with $\partial\tilde{c}_\mathrm{f}/\partial c_\mathrm{s}$ and $\partial\tilde{c}_\mathrm{f}/\partial\pi$, to the parabolicity of the system. In the literature, see e.g. [WW97], it is discussed that potential values for D_c and μ range from 10^{-8}-$10^{-10}\mathrm{m}^2/\mathrm{s}$ and $10^{-4}\mathrm{Pa{\cdot}s}$ while for the permeability κ one finds 10^{-17}-$10^{-14}\mathrm{m}^2$, see e.g. [MI99]. An unprecise tuning of the system might lead to fail the assumption (2.6). This is exemplary seen in Figure **??**, where we have plotted the eigenvalues of $\mathrm{sym}\hat{K} = 1/2(\hat{K} + \hat{K}^\top)$. In the considered range of pressure and concentration it turns out that its smallest eigenvalue is negative whereas the largest eigenvalue is positive. In fact, the uniform positive definiteness of $\hat{K}$, i.e., a lower bound as in (**??**), is equivalent to $\mathrm{sym}\hat{K}$ being positive definite.

As a further difficulty it turns out that the computation of the thermodynamical data set is highly sensitive to the total composition and therefore to the function $\tilde{c}_\mathrm{f}$. This creates approximation errors in the plateau region where $\partial\tilde{c}_\mathrm{f}/\partial c_\mathrm{s} = 0$ that may cause backward diffusion in the system.

Different strategies can be deployed to circumvent this problem: the interpolation of the approximated $\tilde{c}_\mathrm{f}$ function could be constructed to ensure that $\partial\tilde{c}_\mathrm{f}/\partial c_\mathrm{s} = 0 > \delta > 0$. Alternatively, more sophisticated and invasive solutions rely on extensions of the system that account for further geophysical phenomena that could help mitigate this behavior. One possibility is to include more species and phases, which would lead to a change in the landscape of $\tilde{c}_\mathrm{f}$, possibly avoiding a plateau of the previous type. In general, non-convex regions in the energy landscape can produce $\partial\tilde{c}_\mathrm{f}/\partial c_\mathrm{s} = 0$ of different signs, indicating that phase separation is taking place. In such a case, higher-order derivatives as in the Cahn-Hilliard model might help to ensure the mathematical well-posedness of the problem.

2.3 General parabolic system

Collecting the results from subsections 2.1 and 2.2 we see that both systems (1) and (2) can be represented in the form

$$\partial_t \boldsymbol{\rho} - \operatorname{div}\Big(\mathbb{M}(\boldsymbol{\rho})\nabla\boldsymbol{\rho}\Big) = 0\,, \tag{20a}$$

where $\boldsymbol{\rho}$ could be either ρ_tot from (11) with $\mathbb{M} = \hat{K}_\mathrm{D}$ or $\boldsymbol{\rho}$ from (18) with $\mathbb{M} = \hat{\mathbb{M}}$. Both evolutions are assumed to take place on a bounded domain $\Omega \subset \mathbb{R}^d$ with $d = 2, 3$ and with Lipschitz boundary. The systems are then completed with an initial condition

$$\boldsymbol{\rho}(0) = \boldsymbol{\rho}_0\,, \tag{20b}$$

and homogenous Dirichlet boundary conditions on the Dirichlet part Γ_D of the boundary $\partial\Omega$ and inhomogenous Neumann condition on the remaining boundary $\Gamma_\mathrm{N} := \partial\Omega \setminus \Gamma_\mathrm{D}$, i.e.,

$$\boldsymbol{\rho} = 0 \quad \text{ on } (0,\mathrm{T}) \times \Gamma_\mathrm{D}\,, \qquad \mathbb{M}\nabla\boldsymbol{\rho}\cdot\boldsymbol{\nu} = h \quad \text{ on } (0,\mathrm{T}) \times \Gamma_\mathrm{N}\,, \tag{20c}$$

where $\boldsymbol{\nu}$ denotes the outward unit normal to $\partial\Omega$ and the function $h \in L^1(0,\mathrm{T}; H^{-1/2}(\Gamma_\mathrm{N}))$ is time and space dependent. In the same spirit as in the introduction, we can combine the weak formulations (5) and (21) to write a more general weak system for a suitable function space $\boldsymbol{V}$ that could be either V from (4) or $V \times V$:

Definition 2.7. *Let* $\mathrm{T} > 0$ *and* $\Omega \subset \mathbb{R}^d$ *be a bounded Lipschitz domain. Let* $Q_\mathrm{T} := (0,\mathrm{T}) \times \mathbb{R}^d$ *be the time-space cylinder. Given a function* $\boldsymbol{\rho} : [0,\mathrm{T}] \to \boldsymbol{V}$ *we define the following weak formulation for every test function* $\boldsymbol{v} \in \boldsymbol{V}$*:*

$$\int_{Q_\mathrm{T}} \dot{\boldsymbol{\rho}}(t)\, \boldsymbol{v} + \mathbb{M}(\boldsymbol{\rho}(t))\nabla\boldsymbol{\rho}(t) \cdot \nabla \boldsymbol{v} \,\mathrm{d}x\,\mathrm{d}t - \int_0^\mathrm{T} \int_{\Gamma_\mathrm{N}} \boldsymbol{v}|_{\Gamma_\mathrm{N}} h \,\mathrm{d}\mathcal{H}^{d-1}\,\mathrm{d}t = \boldsymbol{0}\,. \tag{21}$$

In the following sections we will study the PDE system (20a). When specific details are needed we will focus our attention on (15) but the reader should keep in mind that slightly readapted results hold also for (11).

2.4 A-priori estimates

From the weak formualtion (21) one can readily obtain some a-priori estimates for the solutions. The first estimates can be obtained by testing (21) with the solution $\boldsymbol{\rho}$:

$$\boldsymbol{0} = \int_0^\mathrm{T} \frac{1}{2}\frac{\mathrm{d}}{\mathrm{d}t}\|\boldsymbol{\rho}(t)\|^2_{L^2(\Omega)}\mathrm{d}t + \int_{Q_\mathrm{T}} \mathbb{M}(\boldsymbol{\rho})|\nabla\boldsymbol{\rho}|^2 \,\mathrm{d}x\mathrm{d}t - \int_0^\mathrm{T}\int_{\Gamma_\mathrm{N}} \boldsymbol{\rho}|_{\Gamma_\mathrm{N}} h \, dH\mathrm{d}t \tag{22}$$

$$\geq \frac{1}{2}\left(\|\boldsymbol{\rho}(\mathrm{T})\|^2_{L^2(\Omega)} - \|\boldsymbol{\rho}(0)\|^2_{L^2(\Omega)}\right) + c^* \int_0^\mathrm{T} \|\nabla\boldsymbol{\rho}\|^2_{L^2(\Omega)}\,\mathrm{d}t - \|h\|_{H^{-1/2}(\Gamma_\mathrm{N})}\|\boldsymbol{\rho}\|_{H^{1/2}(\Gamma_\mathrm{N})}\,, \tag{23}$$

where we have used the assumption on the matrix $\mathbb{M}$ 2.3 and 2.6. From (22) we can infer

$$\|\boldsymbol{\rho}\|_{L^2(0,\mathrm{T};\boldsymbol{V})} \leq C \tag{24a}$$

$$\|\boldsymbol{\rho}\|_{L^\infty(0,\mathrm{T};L^2(\Omega))} \leq C \tag{24b}$$

Further estimates can be obtained by regarding $\partial_t\boldsymbol{\rho}$ as an operator in the dual space $\boldsymbol{V}^*$ and exploiting the boundedness of $\mathbb{M}$:

$$\begin{aligned}
\|\partial_t\boldsymbol{\rho}\|_{L^2(0,\mathrm{T};H^{-1}(\Omega))} &= \sup_{\|\boldsymbol{v}\|_{L^2(0,\mathrm{T};\boldsymbol{V})}\leq 1} \int_0^\mathrm{T} \langle \dot{\boldsymbol{\rho}}, \boldsymbol{v}\rangle_{L^2(\Omega)}\,\mathrm{d}t \\
&= \sup_{\|\boldsymbol{v}\|_{L^2(0,\mathrm{T};\boldsymbol{V})}\leq 1} \int_0^\mathrm{T} \langle \mathbb{M}(\boldsymbol{\rho})\nabla\boldsymbol{\rho}, \nabla\boldsymbol{v}\rangle_{L^2(\Omega)} - \langle h, \boldsymbol{v}\rangle_{L^2(\partial\Omega)}\,\mathrm{d}t \\
&\leq \sup_{\|\boldsymbol{v}\|_{L^2(0,\mathrm{T};\boldsymbol{V})}\leq 1} \int_0^\mathrm{T} \|\mathbb{M}(\boldsymbol{\rho})\nabla\boldsymbol{\rho}\|_{L^2(\Omega)}\|\nabla\boldsymbol{v}\|_{L^2(\Omega)} + \|h\|_{H^{-1/2}(\partial\Omega)}\|\boldsymbol{v}\|_{H^{1/2}(\partial\Omega)}\,\mathrm{d}t \\
&\leq C^*\|\nabla\boldsymbol{\rho}\|_{L^2(0,\mathrm{T};L^2(\Omega))} \leq C\,.
\end{aligned} \tag{24c}$$

3 Existence of fully discrete solutions

The strategy to find solutions for (20) is to consider a fully discrete scheme at first. We use a Galerkin spatial discretisation approach:

Space discretisation: Let $\boldsymbol{V}_n \subset \boldsymbol{V}, n \in \mathbb{N}$, be finite-dimensional subspaces such that $\boldsymbol{V}_{n_1} \subset \boldsymbol{V}_{n_2}$, if $n_1 \leq n_2$ and such that $\bigcup_{n\in\mathbb{N}} \boldsymbol{V}_n \subset \boldsymbol{V}$ densely. Let $(\boldsymbol{e}_j)_{j=1}^n$ be a basis for $\boldsymbol{V}_n$, then each element $\boldsymbol{v} \in \boldsymbol{V}_n$ is represented by $\boldsymbol{v} = \sum_{j=1}^n v_j \boldsymbol{e}_j$ and we write $\vec{v} = (v_j)_{j=1}^n \in \mathbb{R}^n$ for the vector of coefficients.

Time discretisation: Consider a partition $\mathbb{T}_\tau = \{0 = t_\tau^0 < t_\tau^1 \ldots < t_\tau^{N_\tau} = \mathrm{T}\}$ of the time interval $[0,\mathrm{T}]$ with step size $\tau = t_\tau^k - t_\tau^{k-1} = \frac{\mathrm{T}}{N_\tau}$. For a sufficiently smooth function $\boldsymbol{v} : [0,\mathrm{T}] \to \boldsymbol{V}$ we set $\boldsymbol{v}_\tau^k := \boldsymbol{v}(t_\tau^k)$ for all $k \in \{1,\ldots,n\}$ and for $t_\tau^k \in \Pi_\tau$ and we introduce the discrete approximations of time derivatives:

$$\mathrm{D}_\tau \boldsymbol{v}_\tau^k := \frac{\boldsymbol{v}_\tau^k - \boldsymbol{v}_\tau^{k-1}}{\tau}\,. \tag{25}$$

Lastly, for the boundary we use an approximation:

$$h_\tau^k := h(t_\tau^k) \tag{26}$$

and denote by $h_{\tau n}^k$ the restriction of $h_\tau^k \in \boldsymbol{V}^*$ to $\boldsymbol{V}_n$, where we naturally have

$$h_{\tau n}^k \to h_\tau^k \ \text{ strongly in } \boldsymbol{V}^* \ \text{ as } n \to \infty \ \text{ for all } k \in \{1, \dots, N_\tau\} \ \text{ and } \tau > 0 \text{ fixed}. \tag{27}$$

Discrete approximation of (20): We keep the time step size $\tau > 0$ fixed and for the initial data $\boldsymbol{\rho}_0$ from (20b) we set $\boldsymbol{\rho}_\tau^0 = \boldsymbol{\rho}_0$. For all $n \in \mathbb{N}$ let $(\boldsymbol{\rho}_{\tau n}^0)_n$ with $\boldsymbol{\rho}_{\tau n}^0 \in \boldsymbol{V}_n$ be approximations of the intial data such that $\boldsymbol{\rho}_{\tau n}^0 \to \boldsymbol{\rho}_\tau^0$ in $\boldsymbol{V}$ as $n \to \infty$. For each $\tau, n > 0$ fixed, using the discrete initial data our aim is to find for every time step $t_\tau^k \in \Pi_\tau$ solutions $\boldsymbol{\rho}_{\tau n}^k \in \boldsymbol{V}_n$ of the following discrete Galerkin scheme based on the weak formulation (21):

$$\forall \boldsymbol{v}_n \in \boldsymbol{V}_n \qquad \int_\Omega \mathrm{D}_\tau \boldsymbol{\rho}_{\tau n}^k \, \boldsymbol{v}_n \, \mathrm{d}x + \int_\Omega \mathbb{M}(\boldsymbol{\rho}_{\tau n}^k) \nabla \boldsymbol{\rho}_{\tau n}^k \cdot \nabla \boldsymbol{v}_n \, \mathrm{d}x = \int_{\Gamma_\mathrm{N}} h_{\tau n}^k \boldsymbol{v}_n \, \mathrm{d}\mathcal{H}^{d-1}(x) \,. \tag{28}$$

The time discretisation scheme here used is the well known implict Euler scheme. This choice is not only made for analytical reasons but also to follow closely the discretisation schemes used in applications, see i.e., [HVJ22, BJV+20]. We state now the two results of this section, the existence of solutions $\boldsymbol{\rho}_\tau^k$ for the Galerkin scheme (28) and their uniform boundedness with respect to index $n \in \mathbb{N}$, c.f. Propositions 3.1 and 3.3

Proposition 3.1 (Existence of fully discrete solutions)**.** *Let for the system (5) the assumptions 2.1,2.2 and 2.3, or alternatively for (6) let 2.4, 2.5 and 2.6 be satisfied. Furthermore, assume $h \in L^2(0, \mathrm{T}; H^{-1/2}(\Gamma_\mathrm{N}))$. Keep $\tau > 0, k \in \{1, \dots, N_\tau\}$ and $n \in \mathbb{N}$ be fixed. Then, there exists a solution $\boldsymbol{\rho}_\tau^k$ of the Galerkin scheme (28) corresponding to system (21).*

Proof. The Galerkin scheme (28) can be rewritten as a system of non-linear equations for the coefficient vector $\vec{w} \in \mathbb{R}^n$:
Test equation (28) with a basis element $\boldsymbol{e}_j$ for $\boldsymbol{V}_n, j = 1, \dots, n$, recall $\boldsymbol{\rho}_{\tau n}^k = \sum_{i=1}^n \rho_{\tau i}^k \boldsymbol{e}_i$ and multiply by τ to get:

$$0 = \sum_{i=1}^n \int_\Omega (\rho_{\tau i}^k - \rho_{\tau i}^{k-1}) \boldsymbol{e}_i \, \boldsymbol{e}_j + \tau \mathbb{M}(\boldsymbol{\rho}_{\tau n}^k) \rho_{\tau i}^k \nabla \boldsymbol{e}_i \cdot \nabla \boldsymbol{e}_j \, \mathrm{d}x - \int_{\Gamma_\mathrm{N}} \tau h_{\tau i}^k \boldsymbol{e}_i \boldsymbol{e}_j \, \mathrm{d}\mathcal{H}^{d-1}(x) \tag{29}$$

where we wrote $\rho_{\tau i}^k$ instead of $\rho_{\tau n_i}^k$ for sake of simplicity. Observe that (29) is a nonlinear system composed by n equations

$$\boldsymbol{g}(\vec{\rho}_{\tau n}^k) := \mathbb{L} \vec{\rho}_{\tau n}^k + \boldsymbol{f}(\vec{\rho}_{\tau n}^k) = \boldsymbol{0} \,, \tag{30}$$

with the first linear addend deriving from the discretized time derivative and the second nonlinear associated to the gradient and to the boundary terms. We show now that it posesses solution for every fixed τ, k, n. To do so, we exploit the following results:

Proposition 3.2 ([Zei86],Prop. 2.8, p.53)**.** *Consider a system of equations*

$$\boldsymbol{g}(\boldsymbol{z}) = (g_i(\boldsymbol{z}))_{i=1}^n = \boldsymbol{0} \qquad \text{where } \boldsymbol{z} \in \mathbb{R}^n \,. \tag{31}$$

Let $\bar{B}_R(0) := \{\boldsymbol{z} \in \mathbb{R}^n, \|z\| \le R\}$ for fixed $R > 0$ and $\|\cdot\|$ a norm in $\mathbb{R}^n$. Let $g_i : \bar{B}_R(0) \to \mathbb{R}$ be continuous for $i = 1, \dots, n$. Further assume that

$$\boldsymbol{g}(\boldsymbol{z}) \cdot \boldsymbol{z} \ge 0 \qquad \text{for all } \boldsymbol{z} \in \mathbb{R}^n \text{ with } \|\boldsymbol{z}\| = R \,. \tag{32}$$

Then (31) has a solution $\boldsymbol{z}$ with $\|\boldsymbol{z}\| \le R$.

The continuity of $\boldsymbol{g} : \mathbb{R}^n \to \mathbb{R}^n$ follows from the properties of $\mathbb{M}$ 2.3 and 2.6. It remains to check condition (32). For that, we first estimate the linear terms via convexity argument

$$\mathbb{L}\vec{\rho}^k_{\tau n} \cdot \vec{\rho}^k_{\tau n} = \left(\boldsymbol{\rho}^k_{\tau n} - \boldsymbol{\rho}^{k-1}_{\tau n}\right) \cdot \boldsymbol{\rho}^k_{\tau n} \geq (1-\varepsilon)\,|\vec{\rho}^k_{\tau n}|^2 - \varepsilon|\vec{\rho}^{k-1}_{\tau n}|^2\,, \tag{33}$$

with ε arbitrary but such that $\left(1 - \frac{1}{4\varepsilon}\right) > 0$. For the nonlinear term we exploit the positive definitness of $\mathbb{M}$ and Young's argument to get

$$\boldsymbol{f}(\vec{\rho}^k_{\tau n}) \cdot \vec{\rho^k_{\tau n}} = \tau\mathbb{M}(\boldsymbol{\rho}^k_{\tau n})|\nabla\boldsymbol{\rho}^k_{\tau n}|^2 - \tau h^k_{\tau n}\boldsymbol{\rho}^k_{\tau n} \geq \tau c^*|\vec{\rho}^k_{\tau n}|^2 - \tau^2|h^k_{\tau n}|^2 - \frac{1}{4}|\vec{\rho}^k_{\tau n}|^2\,. \tag{34}$$

Together these two estimates lead to

$$\boldsymbol{g}(\vec{\rho}^k_{\tau n}) \cdot \vec{\rho}^k_{\tau n} \geq \left(1 - \frac{1}{4\varepsilon}\right)|\vec{\rho}^k_{\tau n}|^2 - \varepsilon|\vec{\rho}^{k-1}_{\tau n}|^2 + \tau c^*|\vec{\rho}^k_{\tau n}|^2 - \tau^2|h^k_{\tau n}|^2 - \frac{1}{4}|\vec{\rho}^k_{\tau n}|^2\,, \tag{35}$$

which is positive for some $R \geq \sqrt{\frac{4\varepsilon^2}{4\varepsilon(1+\tau c^*)-1-\varepsilon\tau^2}\left(|\vec{\rho}^{k-1}_{\tau n}|^2 + |h^k_{\tau n}|^2\right)}$. □

Similarly to sec. 2.4 we now derive some bound for the fully discrete solutions.

Proposition 3.3 (Uniform a-priori bound for fully discrete solutions)**.** *Let the assumptions of Proposition 3.1 be fulfilled. Furthermore assume that the discrete initial data $(\boldsymbol{\rho}^0_{\tau n})_n$ are uniformly bounded. Then, the fully discrete solution $\boldsymbol{\rho}^k_{\tau n}$ of problem (28) satisfies the following uniform a-priori bound*

$$\|\boldsymbol{\rho}^k_{\tau n}\|_{\boldsymbol{V}} \leq \tilde{C}\,, \tag{36}$$

with a constant $\tilde{C} = \tilde{C}(\boldsymbol{\rho}_0, \tau, C^*, c^*)$ depending on $\boldsymbol{\rho}_0, \tau, C^*, c^*$ but independent of $n \in \mathbb{N}$.

Proof. We procede by induction and see that the assertion is already satisfied for the initial step $k = 0$ thanks to the assumptions on the initial data. For any step $k \in \mathbb{N}$, suppose that $\boldsymbol{\rho}^{k-1}_{\tau n}$ is uniformely bounded in $\boldsymbol{V}$. We test then (28) by the solution $\boldsymbol{\rho}^k_{\tau n}$ and estimate

$$0 = \|\boldsymbol{\rho}^k_{\tau n}\|^2_{L^2(\Omega)} - \int_\Omega \boldsymbol{\rho}^k_{\tau n}\boldsymbol{\rho}^{k-1}_{\tau n}\,\mathrm{d}x + \tau\int_\Omega \mathbb{M}(\boldsymbol{\rho}^k_{\tau n})|\nabla\boldsymbol{\rho}^k_{\tau n}|^2\,\mathrm{d}x - \int_{\Gamma_\mathrm{N}} h^k_{\tau n}\boldsymbol{\rho}^k_{\tau n}\mathrm{d}\mathcal{H}^{d-1}(x) \tag{37}$$

$$\geq \frac{1}{4}\|\boldsymbol{\rho}^k_{\tau n}\|^2_{L^2(\Omega)} - \frac{\|\boldsymbol{\rho}^{k-1}_{\tau n}\|^2_{L^2(\Omega)}}{2} + \tau c^*\|\nabla\boldsymbol{\rho}^k_{\tau n}\|^2_{L^2(\Omega)} - \tau^2\|h^k_{\tau n}\|_{H^{-1/2}(\Gamma_\mathrm{N})}\,, \tag{38}$$

where we have used Young's inequality, the boundedness of $\mathbb{M}$ and the regularity of h. □

4 Limit passage from the space-discrete to space-continuous setting

In this section we keep the time step size $\tau > 0$ fixed and pass to the limit $n \to \infty$ with the space discretisation. We have the following result:

Proposition 4.1 (Existence of solution in the space-continuous setting)**.** *Let the assumptions of 3.1 and 3.3 be satisfied. Let $\boldsymbol{\rho}^k_{\tau n}$ be a solution of (28) for all $\tau > 0, n \in \mathbb{N}$. Then the following convergence results hold true:*

1. *For each $k \in \{1, \dots, N_\tau\}$ there is a (non relabelled) subsequence $(\boldsymbol{\rho}^k_{\tau n})_n$ and a limit value $\boldsymbol{\rho}^k_\tau$ such that*
$$\boldsymbol{\rho}^k_{\tau n} \rightharpoonup \boldsymbol{\rho}^k_\tau \qquad \text{weakly in } \boldsymbol{V}\,, \tag{39}$$
2. *For each $k \in \{1, \dots, N_\tau\}$ the limit value $\boldsymbol{\rho}^k_\tau$ is a solution to the time-discrete problem*
$$\int_\Omega \mathrm{D}_\tau\boldsymbol{\rho}^k_\tau\,\boldsymbol{v} + \mathbb{M}(\boldsymbol{\rho}^k_\tau)\nabla\boldsymbol{\rho}^k_\tau \cdot \nabla\boldsymbol{v}\,\mathrm{d}x - \int_{\Gamma_\mathrm{N}} h^k_\tau\boldsymbol{v}\,\mathrm{d}\mathcal{H}^{d-1}(x) = 0 \qquad \text{for all } \boldsymbol{v} \in \boldsymbol{V}\,. \tag{40}$$

3. *If we assume in addition that the discrete initial data satisfy*

$$\boldsymbol{\rho}_{\tau n}^0 \to \boldsymbol{\rho}_\tau^0 \qquad \text{in } \boldsymbol{V}\,, \tag{41}$$

Then, in addition to (39) *for each* $k \in \{1, \dots, N_\tau\}$ *the following improved convergence also holds true:*

$$\boldsymbol{\rho}_{\tau n}^k \to \boldsymbol{\rho}_\tau^k \qquad \text{strongly in } \boldsymbol{V}\,. \tag{42}$$

Proof. 1. This is a direct consequence of the uniform a-priori bound (36).

2. In order to pass to the limit $n \to \infty$ in (28) we let $\boldsymbol{v} \in \boldsymbol{V}$ be a test function of the space-continuous limit problem (40) and $(\boldsymbol{v}_n)_n \subset \boldsymbol{V}$ such that $\boldsymbol{v}_n \in \boldsymbol{V}_n$ for all $n \in \mathbb{N}$ are test functions for the finite dimensional problem (28) with the property $\boldsymbol{v}_n \to \boldsymbol{v}$ strongly in $\boldsymbol{V}$. We recall that a sequence $(\boldsymbol{v}_n)_n$ with these property exists since, by construction, $\bigcup_{n\in\mathbb{N}} \boldsymbol{V}_n$ is dense in $\boldsymbol{V}$. Now for the limit passage in (28) we have

$$\tfrac{1}{\tau}\int_\Omega (\boldsymbol{\rho}_{\tau n}^k - \boldsymbol{\rho}_{\tau n}^{k-1})\,\boldsymbol{v}_n + \mathbb{M}(\boldsymbol{\rho}_{\tau n}^k)\nabla\boldsymbol{\rho}_{\tau n}^k \cdot \nabla\boldsymbol{v}_n \,\mathrm{d}x - \int_{\Gamma_{\mathrm{N}}} h_{\tau n}^k \boldsymbol{v}_n \,\mathrm{d}\mathcal{H}^{d-1}(x) = 0\,.$$

The first addend convergence is ensured by weak convergence of $\boldsymbol{\rho}_{\tau n}^k$ (39) and strong convergence of the test functions $\boldsymbol{v}_n$ in $\boldsymbol{V}$. Strong convergence of the test functions together with the strong convergence $h_{\tau n}^k \to h_\tau^k$ in $\boldsymbol{V}^*$, implies convergence of the boundary term. For the second bulk term we exploit the compact embedding of $\boldsymbol{V}$ into $L^2(\Omega)$ to find a strongly convergent subsequence and from that a further strongly a.e. pointwise converging subsequence (not relabelled),

$$\boldsymbol{\rho}_{\tau n}^k(x) \to \boldsymbol{\rho}_\tau^k(x) \qquad \text{for a.e. } x \in \Omega\,.$$

Then by continuity of $\mathbb{M}$ there follows

$$\mathbb{M}(\boldsymbol{\rho}_{\tau n}^k)\nabla\boldsymbol{v}_n(x) \to \mathbb{M}(\boldsymbol{\rho}_\tau^k)\nabla\boldsymbol{v}(x) \qquad \text{for a.e. } x \in \Omega\,.$$

Exploiting the boundedness of $\mathbb{M}$ and $\nabla\boldsymbol{v}_n \to \nabla\boldsymbol{v}$ in $L^2(\Omega)$, we conclude by dominated convergence theorem that

$$\mathbb{M}(\boldsymbol{\rho}_{\tau n}^k)\nabla\boldsymbol{v}_n \to \mathbb{M}(\boldsymbol{\rho}_\tau^k)\nabla\boldsymbol{v} \qquad \text{strongly in } L^2(\Omega)\,,$$

which, together with the weak convergence of $\nabla\boldsymbol{\rho}_{\tau n}^k \rightharpoonup \nabla\boldsymbol{\rho}_\tau^k$, implies convergence of the second addend. Check this proof for new BC

3. By induction assume that at the previous time step we have $\boldsymbol{\rho}_{\tau n}^{k-1} \to \boldsymbol{\rho}_\tau^{k-1}$ in $\boldsymbol{V}$. From the weak convergence $\boldsymbol{\rho}_{\tau n}^{k-1} \rightharpoonup \boldsymbol{\rho}_\tau^{k-1}$ in $\boldsymbol{V}$ we can extract a (non-relabelled) subsequence $\boldsymbol{\rho}_{\tau n}^{k-1} \to \boldsymbol{\rho}_\tau^{k-1}$ in $L^2(\Omega)$ then we test (28) with the solution $\boldsymbol{\rho}_{\tau n}^k$ and get

$$\int_\Omega \mathbb{M}(\boldsymbol{\rho}_{\tau n}^k)|\nabla\boldsymbol{\rho}_{\tau n}^k|^2 \,\mathrm{d}x = \frac{1}{\tau}\int_\Omega -|\boldsymbol{\rho}_{\tau n}^k|^2 + \boldsymbol{\rho}_{\tau n}^k\boldsymbol{\rho}_{\tau n}^{k-1} \,\mathrm{d}x + \int_{\Gamma_{\mathrm{N}}} h_{\tau n}^k \boldsymbol{\rho}_{\tau n}^k \,\mathrm{d}\mathcal{H}^{d-1}(x)\,.$$

Convergence of the right hand side is given by weak-strong argument, while for the left hand side we apply [Dac07, Thm 3.4, pp. 74] and get

$$\begin{aligned}
\int_\Omega \mathbb{M}(\boldsymbol{\rho}_{\tau n}^k)|\nabla\boldsymbol{\rho}_{\tau n}^k|^2 \,\mathrm{d}x &\le \liminf_{n\to\infty} \int_\Omega \mathbb{M}(\boldsymbol{\rho}_{\tau n}^k)|\nabla\boldsymbol{\rho}_{\tau n}^k|^2 \,\mathrm{d}x \\
&\le \limsup_{n\to\infty} \int_\Omega \mathbb{M}(\boldsymbol{\rho}_{\tau n}^k)|\nabla\boldsymbol{\rho}_{\tau n}^k|^2 \,\mathrm{d}x \\
&= \lim_{n\to\infty} \frac{1}{\tau}\int_\Omega -|\boldsymbol{\rho}_{\tau n}^k|^2 + \boldsymbol{\rho}_{\tau n}^k\boldsymbol{\rho}_{\tau n}^{k-1} \,\mathrm{d}x + \int_{\Gamma_{\mathrm{N}}} h_{\tau n}^k \boldsymbol{\rho}_{\tau n}^k \,\mathrm{d}\mathcal{H}^{d-1}(x) \\
&= \frac{1}{\tau}\int_\Omega -|\boldsymbol{\rho}_\tau^k|^2 + \boldsymbol{\rho}_\tau^k\boldsymbol{\rho}_\tau^{k-1} \,\mathrm{d}x + \int_{\Gamma_{\mathrm{N}}} h_\tau^k \boldsymbol{\rho}_\tau^k \,\mathrm{d}\mathcal{H}^{d-1}(x) \\
&= \int_\Omega \mathbb{M}(\boldsymbol{\rho}_\tau^k)|\nabla\boldsymbol{\rho}_\tau^k|^2 \,\mathrm{d}x\,.
\end{aligned}$$

Then introduce the projection operator $\mathbb{P}_n : \boldsymbol{V} \to \boldsymbol{V}_n$ that maps space continuous into space discrete functions and by Korn's inequality and boundedness of $\mathbb{M}$ we can conclude

$$\begin{aligned}
C_k^2\|\boldsymbol{\rho}_{\tau n}^k - \boldsymbol{\rho}_\tau^k\|_{\boldsymbol{V}}^2 &\leq \|\nabla\boldsymbol{\rho}_{\tau n}^k - \nabla\boldsymbol{\rho}_\tau^k\|_{L^2(\Omega)}^2 \\
&\leq 2\|\nabla\boldsymbol{\rho}_{\tau n}^k - \nabla\mathbb{P}_n(\boldsymbol{\rho}_\tau^k)\|_{L^2(\Omega)}^2 + 2\|\nabla\mathbb{P}_n(\boldsymbol{\rho}_\tau^k) - \nabla\boldsymbol{\rho}_\tau^k\|_{L^2(\Omega)}^2 \\
&\leq \tfrac{2}{c^*}\int_\Omega \mathbb{M}(\boldsymbol{\rho}_{\tau n}^k)|\nabla\boldsymbol{\rho}_{\tau n}^k - \nabla\mathbb{P}_n(\boldsymbol{\rho}_\tau^k)|^2\mathrm{d}x + 2\|\nabla\mathbb{P}_n(\boldsymbol{\rho}_\tau^k) - \nabla\boldsymbol{\rho}_\tau^k\|_{L^2(\Omega)}^2 \\
&= \tfrac{2}{c^*}\int_\Omega \mathbb{M}(\boldsymbol{\rho}_{\tau n}^k)|\boldsymbol{\rho}_{\tau n}^k|^2\,\mathrm{d}x - \tfrac{4}{c^*}\int_\Omega \mathbb{M}(\boldsymbol{\rho}_{\tau n}^k)\nabla\boldsymbol{\rho}_{\tau n}^k\cdot\mathbb{P}_n(\boldsymbol{\rho}_\tau^k)\,\mathrm{d}x \\
&+ \tfrac{2}{c^*}\int_\Omega \mathbb{M}(\boldsymbol{\rho}_{\tau n}^k)|\nabla\mathbb{P}_n(\boldsymbol{\rho}_\tau^k)|^2\,\mathrm{d}x + 2\|\nabla\mathbb{P}_n(\boldsymbol{\rho}_\tau^k) - \nabla\boldsymbol{\rho}_\tau^k\|_{L^2(\Omega)}^2 \to 0\,.
\end{aligned}$$

□

For space-continuous time-discrete solutions $(\boldsymbol{\rho}_\tau^k)_{k=1}^{N_\tau}$ of (40), it is possible to define piecewise constant interpolants $\bar{\boldsymbol{\rho}}_\tau, \underline{\boldsymbol{\rho}}_\tau$, and affine-linear approximation $\boldsymbol{\rho}_\tau$ for $t \in (t_\tau^{k-1}, t_\tau^k], k = 1, \dots, N_\tau$

$$\bar{\boldsymbol{\rho}}_\tau(t) := \boldsymbol{\rho}_\tau^k\,, \quad \underline{\boldsymbol{\rho}}_\tau(t) := \boldsymbol{\rho}_\tau^{k-1}\,, \quad \boldsymbol{\rho}_\tau(t) := \frac{t - t_\tau^{k-1}}{\tau}\boldsymbol{\rho}_\tau^k + \frac{t_\tau^k - t}{\tau}\boldsymbol{\rho}_\tau^{k-1}\,, \tag{43}$$

and similarly for the external forces $\hat{h} \in \{h_\tau, \bar{h}_\tau, \underline{h}_\tau\}$ and we set for any $t \in (t_\tau^{k-1}, t_\tau^k]$

$$\bar{t}_\tau(t) := t_\tau^k\,.$$

In this way we can write a time-continuous weak formulation of the time-discrete problem (40)

$$\int_0^{\bar{t}_\tau(t)}\int_\Omega \dot{\boldsymbol{\rho}}_\tau(r)\boldsymbol{v}(r) + \mathbb{M}(\boldsymbol{\rho}_\tau(r))\nabla\boldsymbol{\rho}_\tau(r)\cdot\nabla\boldsymbol{v}(r)\,\mathrm{d}x - \int_{\Gamma_{\mathrm{N}}} h_\tau(r)\boldsymbol{v}(r)\,\mathrm{d}\mathcal{H}^{d-1}(x)\,\mathrm{d}r = 0 \tag{44}$$

We can now find bounds for the interpolants defined above that will used later on for the limit passage from time-discrete to time-continuous.

Proposition 4.2 (Uniform a-priori bounds for time-discrete solutions)**.** *Let the assumptions of 4.1 be satisfied and in addition set $\boldsymbol{\rho}_\tau^0 = \boldsymbol{\rho}_0$. For the interpolants constructed by (43) with the time-discrete limit value found in (39) the following a-priori estimates hold true with a constant $C > 0$ independent of τ:*

$$\|\bar{\boldsymbol{\rho}}_\tau\|_{B(0,\mathrm{T};L^2(\Omega))} + \|\underline{\boldsymbol{\rho}}_\tau\|_{B(0,\mathrm{T};L^2(\Omega))} + \|\boldsymbol{\rho}_\tau\|_{B(0,\mathrm{T};L^2(\Omega))} \leq C\,, \tag{45a}$$

$$\|\boldsymbol{\rho}_\tau\|_{L^2(0,\mathrm{T};\boldsymbol{V})} \leq C\,, \tag{45b}$$

$$\|\dot{\boldsymbol{\rho}}_\tau\|_{L^2(0,\mathrm{T};\boldsymbol{V}^*)} \leq C\,, \tag{45c}$$

Proof. The estimates (45a) and (45b) are obtained by testing (40) with the space-continuous solution $\boldsymbol{\rho}_\tau^k$

$$\begin{aligned}
0 &= \int_\Omega (\boldsymbol{\rho}_\tau^k - \boldsymbol{\rho}_\tau^{k-1})\,\boldsymbol{\rho}_\tau^k\,\mathrm{d}x + \tau\int_\Omega \mathbb{M}(\boldsymbol{\rho}_\tau^k)|\nabla\boldsymbol{\rho}_\tau^k|^2\,\mathrm{d}x - \tau\int_{\Gamma_{\mathrm{N}}} h_\tau^k\boldsymbol{\rho}_\tau^k\,\mathrm{d}\mathcal{H}^{d-1}(x) \\
&\geq \int_\Omega |\boldsymbol{\rho}_\tau^k|^2 - \boldsymbol{\rho}_\tau^{k-1}\boldsymbol{\rho}_\tau^k\,\mathrm{d}x + \tau c^*\int_\Omega |\nabla\boldsymbol{\rho}_\tau^k|^2\,\mathrm{d}x - \tfrac{8}{9}\|\boldsymbol{\rho}_\tau^k\|_{L^2(\Omega)}^2 - \tau^2\|h_\tau^k\|_{H^{-1/2}(\Gamma_{\mathrm{N}})}^2 \\
&\geq \tfrac{1}{4}\|\boldsymbol{\rho}_\tau^k\|_{L^2(\Omega)}^2 - \tfrac{1}{2}\|\boldsymbol{\rho}_\tau^{k-1}\|_{L^2(\Omega)}^2 + \tau c^*\|\nabla\boldsymbol{\rho}_\tau^k\|_{L^2(\Omega)}^2 - \tau^2\|h_\tau^k\|_{H^{-1/2}(\Gamma_{\mathrm{N}})}^2
\end{aligned}$$

where we have used Young's inequality and exploited the positive definitness of $\mathbb{M}$. From this we infer (45a). On the other hand, this inequality holds true for all $k \in \{1, \dots, N_\tau\}$ and thus by summing over all indeces we get a telescopic sum which ultimetly results in

$$\tfrac{1}{2}\|\boldsymbol{\rho}_\tau^0\|_{L^2(\Omega)}^2 + C_h \geq \tfrac{1}{2}\|\boldsymbol{\rho}_\tau^{N_\tau}\|_{L^2(\Omega)}^2 + c^*\int_0^{\mathrm{T}} \|\nabla\boldsymbol{\rho}_\tau\|_{L^2\Omega}^2(t)\,\mathrm{d}t\,,$$

where $C_h > 0$ is constant related to h and depend on T. By the assumptions on the initial data we conclude (45b). For (45c) we regard $\dot{\boldsymbol{\rho}}_\tau$ as an operator acting in the dual space $\boldsymbol{V}^*$

$$\begin{aligned}
\|\dot{\boldsymbol{\rho}}_\tau\|_{L^2(0,T;\boldsymbol{V}^*)} &= \sup_{\|\boldsymbol{v}\|_{L^2(0,\mathrm{T};\boldsymbol{V})}\leq 1} \int_0^{\mathrm{T}} \langle \dot{\boldsymbol{\rho}}_\tau, \boldsymbol{v}\rangle_{L^2(\Omega)}\,\mathrm{d}t \\
&= \sup_{\|\boldsymbol{v}\|_{L^2(0,\mathrm{T};\boldsymbol{V})}\leq 1} \int_0^{\mathrm{T}} \langle \mathbb{M}(\boldsymbol{\rho}_\tau)\nabla\boldsymbol{\rho}_\tau, \nabla\boldsymbol{v}\rangle_{L^2(\Omega)} - \langle h, \boldsymbol{v}\rangle_{H^{1/2}(\Gamma_{\mathrm{N}})}\,\mathrm{d}t \\
&\leq \sup_{\|\boldsymbol{v}\|_{L^2(0,\mathrm{T};\boldsymbol{V})}\leq 1} \int_0^{\mathrm{T}} \|\mathbb{M}(\boldsymbol{\rho}_\tau)\nabla\boldsymbol{\rho}_\tau\|_{L^2(\Omega)}\|\nabla\boldsymbol{v}\|_{L^2(\Omega)} - \|h\|_{H^{-1/2}(\Gamma_{\mathrm{N}})}\|\boldsymbol{v}\|_{H^{1/2}(\Gamma_{\mathrm{N}})}\,\mathrm{d}t \\
&\leq C^*\|\nabla\boldsymbol{\rho}_\tau\|_{L^2(0,\mathrm{T};L^2(\Omega))} \leq C\,.
\end{aligned}$$

□

5 Limit passage from the time-discrete to the time-continuous setting

In this section we perform a limit passage $\tau \to 0$ (from time-discrete to time-continuous) for the interpolants $\bar{\boldsymbol{\rho}}_\tau, \underline{\boldsymbol{\rho}}_\tau$ and $\boldsymbol{\rho}_\tau$.

Theorem 5.1 (Existence of solutions)**.** *Let the assumptions of Propositions 4.1-4.2 be satisfied. Then, the following statements hold true:*

1. *There exists a function $\boldsymbol{\rho} : [0,\mathrm{T}] \to \boldsymbol{V}$ such that the following convergence statements are valid:*

$$\begin{aligned}
\bar{\boldsymbol{\rho}}_\tau, \underline{\boldsymbol{\rho}}_\tau, \boldsymbol{\rho}_\tau &\overset{*}{\rightharpoonup} \boldsymbol{\rho} && \text{weakly-}* \text{ in } L^\infty(0,\mathrm{T};L^2(\Omega))\,, && (46a)\\
\bar{\boldsymbol{\rho}}_\tau, \boldsymbol{\rho}_\tau &\rightharpoonup \boldsymbol{\rho} && \text{weakly in } L^2(0,\mathrm{T};\boldsymbol{V})\,, && (46b)\\
\bar{\boldsymbol{\rho}}_\tau, \boldsymbol{\rho}_\tau &\to \boldsymbol{\rho} && \text{strongly in } L^2(0,\mathrm{T};L^2(\Omega))\,, && (46c)\\
\dot{\boldsymbol{\rho}}_\tau &\rightharpoonup \boldsymbol{u} && \text{weakly in } L^2(0,\mathrm{T};\boldsymbol{V}^*)\,, && (46d)\\
\bar{\boldsymbol{\rho}}_\tau(t), \underline{\boldsymbol{\rho}}_\tau(t), \boldsymbol{\rho}_\tau(t) &\overset{*}{\rightharpoonup} \boldsymbol{\rho}(t) && \text{weakly-}* \text{ in } \boldsymbol{V}^* \quad \text{for all } t\in[0,\mathrm{T}]\,, && (46e)
\end{aligned}$$

2. *The limiting function $\boldsymbol{\rho}$ has the regularity*

$$\boldsymbol{\rho} \in H^1(0,\mathrm{T};\boldsymbol{V}^*)\cap L^2(0,\mathrm{T};\boldsymbol{V})\cap L^\infty(0,\mathrm{T};L^2(\Omega))\cap C^0([0,\mathrm{T}];L^2(\Omega))\,, \tag{47}$$

and satisfies the weak formulation

$$\int_{Q_{\mathrm{T}}} \dot{\boldsymbol{\rho}}(t)\,\boldsymbol{v}(t) + \mathbb{M}(\boldsymbol{\rho}(t))\nabla\boldsymbol{\rho}(t)\cdot\nabla\boldsymbol{v}(t)\,\mathrm{d}x\,\mathrm{d}t - \int_0^{\mathrm{T}}\int_{\Gamma_{\mathrm{N}}} \boldsymbol{v}(t)|_{\Gamma_{\mathrm{N}}}\mathbb{M}(\boldsymbol{\rho}(t))\nabla\boldsymbol{\rho}(t)\cdot\nu\,\mathrm{d}\mathcal{H}^{d-1}(x)\,\mathrm{d}t = \mathbf{0} \tag{48}$$

for all $\boldsymbol{v}\in L^2(0,\mathrm{T};\boldsymbol{V})$ and $\boldsymbol{\rho}(0) = \boldsymbol{\rho}_0$.

Proof. 1. From (45a),(45c) and compactness arguments we get (46a), (46d) and by duality argument

$$\boldsymbol{\rho}_\tau \rightharpoonup \boldsymbol{\rho} \qquad \text{weakly in } L^1(0,\mathrm{T};L^2(\Omega))\,. \tag{49}$$

From (45b) we get that there exists a subsequence (not relabelled) such that:

$$\boldsymbol{\rho}_\tau \rightharpoonup \boldsymbol{\rho} \qquad \text{weakly in } L^2(0,\mathrm{T};\boldsymbol{V})\,, \tag{50}$$

where the limit coincides with the one in (49) because of the space inclusion. From (45c) and the definition of discrete time derivative $\mathrm{D}_\tau \boldsymbol{\rho}_\tau^k = \frac{\boldsymbol{\rho}_\tau^k - \boldsymbol{\rho}_\tau^{k-1}}{\tau}$ we have the estimate

$$\|\boldsymbol{\rho}_\tau\|_{BV(0,\mathrm{T};\boldsymbol{V}^*)} \leq C\,. \tag{51}$$

We apply then [MR15, thm. B.5.10] and find a subsequence

$$\boldsymbol{\rho}_\tau(t) \overset{*}{\rightharpoonup} \tilde{\boldsymbol{\rho}}(t) \qquad \text{weakly-}* \text{ in } \boldsymbol{V}^*\text{, for every } t \in [0,\mathrm{T}]\,,$$

with $\tilde{\boldsymbol{\rho}} \in BV(0,\mathrm{T};\boldsymbol{V}^*)$. Then, [DJ12, thm. 1] with the compact embedding $L^2(\Omega) \subset\subset \boldsymbol{V}^*$ and $\boldsymbol{V} \subset\subset L^2(\Omega)$, a version of Aubin-Lions compactness argument adapted to time-discretization and piecewise constant sequences in time $(\boldsymbol{\rho}_\tau)_\tau$ can be used to find for this subsequence

$$\begin{aligned} &\boldsymbol{\rho}_\tau \to \hat{\boldsymbol{\rho}} && \text{strongly in } L^p(0,\mathrm{T};\boldsymbol{V}^*) \text{ with } p \in [1,\infty)\,,\\ &\boldsymbol{\rho}_\tau \to \check{\boldsymbol{\rho}} && \text{strongly in } L^2(0,\mathrm{T};L^2(\Omega))\,, \end{aligned}$$

with $\check{\boldsymbol{\rho}} \in C^0([0,\mathrm{T}];\boldsymbol{V}^*)$. Strong convergence implies the existence of a (not relabelled) subsequence weakly convergent

$$\boldsymbol{\rho}_\tau(t) \rightharpoonup \check{\boldsymbol{\rho}}(t) \qquad \text{weakly in } L^2(\Omega) \text{ for a.e. } t \in [0,\mathrm{T}]$$

from which we get $\boldsymbol{\rho} = \check{\boldsymbol{\rho}} = \tilde{\boldsymbol{\rho}} = \hat{\boldsymbol{\rho}}$ in $L^2(0,\mathrm{T};\boldsymbol{V}^*)$.

2. Let

$$\boldsymbol{v} \in L^2(0,\mathrm{T};\boldsymbol{V})$$

be a test function for the weak equation (21). We define

$$\boldsymbol{v}_\tau^k := \frac{1}{\tau}\int_{t_\tau^{k-1}}^{t_\tau^k} \boldsymbol{v}(r)\,\mathrm{d}t$$

and set the interpolants as defined in (43). Based on this, there holds

$$\bar{\boldsymbol{v}}_\tau\,, \boldsymbol{v}_\tau \to \boldsymbol{v} \qquad \text{strongly in } L^2(0,\mathrm{T};\boldsymbol{V})\,. \tag{53}$$

In the time-discrete equation (44) the velocity term converges then thanks to (46d) and with a weak-strong convergence argument

$$\int_0^{\bar{t}_\tau(t)}\int_\Omega \dot{\boldsymbol{\rho}}_\tau(r)\boldsymbol{v}(r)\,\mathrm{d}x\,\mathrm{d}r \to \int_0^t\int_\Omega \boldsymbol{u}(r)\boldsymbol{v}(r)\,\mathrm{d}x\,\mathrm{d}r\,.$$

Now if we assume $\boldsymbol{v}$ to be regular enough and use an integration by-part formula suited for Bochner spaces [Rou13, Lemma 7.3, p.205]

$$\int_0^t\int_\Omega \dot{\boldsymbol{\rho}}(r)\boldsymbol{v}(r)\,\mathrm{d}x\,\mathrm{d}r = \int_\Omega (\boldsymbol{\rho}(t)\boldsymbol{v}(t) - \boldsymbol{\rho}(0)\boldsymbol{v}(0))\,\mathrm{d}x - \int_0^t\int_\Omega \boldsymbol{\rho}(r)\dot{\boldsymbol{v}}(r)\,\mathrm{d}x\,\mathrm{d}r\,,$$

we conclude $\dot{\boldsymbol{\rho}} = \boldsymbol{u}$ in the sense of distribution. Additionally, the initial datum is attained, i.e., $\boldsymbol{\rho}(0) = \boldsymbol{\rho}_0$ since by construction we set $\boldsymbol{\rho}_\tau(0) = \boldsymbol{\rho}(0)$ and by (46e) we have $\boldsymbol{\rho}_\tau(0) \overset{*}{\rightharpoonup} \boldsymbol{\rho}(0)$ in $\boldsymbol{V}^*$. Convergence of the boundary term derives from (53) and strong convergence $h_\tau \to h$ in $L^2(0,\mathrm{T};\boldsymbol{V})$. For the remaning term, we recall the continuity of $\mathbb{M}$, cf. 2.3,2.6, the strong convergence of test functions (53) and (46c) imply

$$|\mathbb{M}(\boldsymbol{\rho}_\tau(t))\nabla\boldsymbol{v}_\tau(t)| \to |\mathbb{M}(\boldsymbol{\rho}(t))\nabla\boldsymbol{v}(t)| \qquad \text{for a.e. } t \in [0,\mathrm{T}]\,.$$

Then, exploiting the boundedness of $\mathbb{M}$, we can apply the dominated convergence theorem to deduce

$$\mathbb{M}(\boldsymbol{\rho}_\tau)\nabla\boldsymbol{v}_\tau \to \mathbb{M}(\boldsymbol{\rho})\nabla\boldsymbol{v} \qquad \text{strongly in } L^2(0,\mathrm{T};L^2(\Omega))\,.$$

This result together with the weak convergence (46b) allow us to conclude

$$\int_0^{\bar{t}_\tau(t)}\int_\Omega \mathbb{M}(\boldsymbol{\rho}_\tau(r))\nabla\boldsymbol{\rho}_\tau(r)\cdot\nabla\boldsymbol{v}_\tau(r)\,\mathrm{d}x\,\mathrm{d}r \to \int_0^t\int_\Omega \mathbb{M}(\boldsymbol{\rho}(r))\nabla\boldsymbol{\rho}(r)\cdot\nabla\boldsymbol{v}(r)\,\mathrm{d}x\,\mathrm{d}r\,.$$

3. Regularity of the solutions follows from the convergence statements (46).

□

References

[BJV+20] Andreas Beinlich, Timm John, Johannes C Vrijmoed, Masako Tominaga, Tomas Magna, and Yuri Y Podladchikov. Instantaneous rock transformations in the deep crust driven by reactive fluid flow. *Nature Geoscience*, 13(4):307–311, 2020.

[Dac07] Bernard Dacorogna. *Direct methods in the calculus of variations*, volume 78. Springer Science & Business Media, 2007.

[DJ12] Michael Dreher and Ansgar Jüngel. Compact families of piecewise constant functions in lp (0, t; b). *Nonlinear Analysis: Theory, Methods & Applications*, 75(6):3072–3077, 2012.

[Guy93] Bernard Guy. Mathematical revision of korzhinskii's theory of infiltration metasomatic zoning. *European Journal of Mineralogy*, 5(2):317–339, 1993.

[HVJ22] Konstantin Huber, Johannes C Vrijmoed, and Timm John. Formation of olivine veins by reactive fluid flow in a dehydrating serpentinite. *Geochemistry, Geophysics, Geosystems*, 23(6):e2021GC010267, 2022.

[MI99] Craig E. Manning and Steven E. Ingebritsen. Permeability of the continental crust: Implications of geothermal data and metamorphic systems. *Reviews of Geophysics*, 37(1):127–150, 1999.

[MR15] Alexander Mielke and Tomáš Roubíček. *Rate-Independent Systems: Theory and Application.* Springer New York, 2015.

[PJP+17] Oliver Plümper, Timm John, Yuri Y Podladchikov, Johannes C Vrijmoed, and Marco Scambelluri. Fluid escape from subduction zones controlled by channel-forming reactive porosity. *Nature Geoscience*, 10(2):150–156, 2017.

[Rou13] Tomáš Roubíček. *Nonlinear partial differential equations with applications*, volume 153. Springer Science & Business Media, 2013.

[vKHSA11] Peter E van Keken, Bradley R Hacker, Ellen M Syracuse, and Geoff A Abers. Subduction factory: 4. depth-dependent flux of h2o from subducting slabs worldwide. *Journal of Geophysical Research: Solid Earth*, 116(B1), 2011.

[VP22] Johannes Christiaan Vrijmoed and Yuri Yurivech Podladchikov. Thermolab: A thermodynamics laboratory for nonlinear transport processes in open systems. *Geochemistry, Geophysics, Geosystems*, 23(4):e2021GC010303, 2022.

[WW97] E. Bruce Watson and David A. Wark. Diffusion of dissolved sio2 in h2o at 1 gpa, with implications for mass transport in the crust and upper mantle. *Contributions to Mineralogy and Petrology*, 130(1):66–80, 1997.

[Zei86] Eberhard Zeidler. *Nonlinear Functional Analysis and its Applications I: Fixed-Point Theorems.* Springer-Verlag New York, 1986.

[ZHP+22] Andrea Zafferi, Konstantin Huber, Dirk Peschka, Johannes Vrijmoed, John Timm, and Marita Thomas. A porous-media model for reactive fluid-rock interaction. *CRC1114*, 2022.